ACIBADEM MEHMET ALI AYDINLAR UNIVERSITY
INSTITUTE OF NATURAL AND APPLIED SCIENCES

PREPARATION OF A TISSUE ENGINEERED ANTERIOR CRUCIATE LIGAMENT (ACL) BY ELECTROSPINNING

SELEN EGE KIRBAŞ

M.Sc. THESIS

DEPARTMENT OF BIOMEDICAL ENGINEERING

SUPERVISOR
Prof. Dr. Vasıf HASIRCI

CO-SUPERVISOR
Asst. Prof. Dr. Deniz YÜCEL

ISTANBUL-2023

ACIBADEM MEHMET ALI AYDINLAR UNIVERSITY
INSTITUTE OF NATURAL AND APPLIED SCIENCES

PREPARATION OF A TISSUE ENGINEERED ANTERIOR CRUCIATE LIGAMENT (ACL) BY ELECTROSPINNING

SELEN EGE KIRBAŞ

M.Sc. THESIS

DEPARTMENT OF BIOMEDICAL ENGINEERING

SUPERVISOR
Prof. Dr. Vasıf HASIRCI

CO-SUPERVISOR
Asst. Prof. Dr. Deniz YÜCEL

ISTANBUL-2023

DECLARATION

I declare that this thesis work is my own work, I had no unethical behavior at any stage from the planning to the writing of the thesis, I obtained all the information in this thesis in accordance with academic and ethical rules, I cited all the information and comments that were not obtained with this thesis work, and I provided resources in the list of references. I also declare that there was no violation of any patents and copyrights during the study and writing of this thesis.

18/05/2023

Selen Ege Kırbaş

PREFACE AND ACKNOWLEDGEMENT

I would like to give my deepest gratitude to my supervisor Prof. Dr. Vasıf HASIRCI for his guidance, insight and encouragement. It is through his patience and support throughout my thesis that I was able to complete it.

I would like to thank my co-advisor Asst. Dr. Deniz YÜCEL for her guidance and support throughout this thesis.

I would like to express my deepest gratitude to Prof. Dr. Halime KENAR for her suggestions and her kindness.

I would like to thank the labmates that I had the chance to meet in ACU Biomaterials Center throughout this thesis who had shown me endless support and help.

A big thank you to Aslıhan Akalınlı, Barışcan Uzunkaya, Şeyma Işık[2] and Tuğçe Doğruel for their care, support, understanding and friendship.

I would like to thank Gözde Ervin KÖLE, Deniz BAŞÖZ and Neval SEVİNÇ ÖZDEMİR for their help in teaching me cell culture and electrospinning.

During this study, I was supported by TUBITAK 121N817 and this scholarship is gratefully acknowledged.

I would like to thank my friends, Selay ENDER, Finesa XHIBO, Sedanur KABADAYI, Lorena IMERAJ and Fatma ASLAN who had been there for me and had my back since day one. Without your support and friendship, I would not be here.

Finally, I would like to give my mother Asuman ŞEN and my aunts, Emine ŞEN and Yasemin ŞEN the biggest thanks I can give for their encouragement and for their love. I would also like to thank my father Abdullah KIRBAŞ, for his selfless help and support.

TABLE OF CONTENTS

LIST OF ABBREVIATIONS/ SYMBOLS

ACL Anterior cruciate ligament

US United States

GelMA Methacrylated gelatin

3D Three dimensional

PLA Poly(lactic acid)

MCL Medial collateral ligament

LCL Lateral collateral ligament

PCL Posterior cruciate ligament

AMB Anteromedial bundle

PLB Posteromedial bundle

ECM Extracellular matrix

MRI Magnetic Resonance Imaging

BTB Bone-patellar tendon-bone

PET Poly(ethylene terephthalate)

PTFE Poly(tetrafluoroethylene)

LARS Ligament Advanced Reinforcement System

LAD Ligament Augmentation Device

PCL Poly(ε-caprolactone)

HFIP (1, 1, 1, 3, 3, 3)-Hexafluoro-2-propanol

LAP Lithium phenyl-2,4,6-trimethyl-benzoylphosphinate

TEMED N, N, N', N'-Tetramethyl-ethylene diamine

APS Ammonium persulfate

FITC Fluorescein isothiocyanate

DMEM Dulbecco's Modified Eagle Medium

FBS Fetal Bovine Serum

DMSO Dimethyl sulfoxide

PBS Phosphate buffered saline

SDS-PAGE Sodium Dodecyl Sulfate- Polyacrylamide Gel Electrophoresis

dH_2O Distilled water

SF Silk fibroin

Col Collagen

PEG Polyethylene glycol

SEM Scanning Electron Microscopy

DPBS Dulbecco's Phosphate Buffered Saline

^{1}H-NMR ^{1}H-Nuclear Magnetic Resonance

D_2O Heavy water/deuterium oxide

MD Methacrylation Degree

UV Ultraviolet

EWC Equilibrium Water Content

P/S/A Penicillin/Streptomycin/Amphotericin-B

EtOH Ethanol

CLSM Confocal Laser Scanning Microscopy

DAPI 4',6-Diamino-2-phenylindole

PFA Paraformaldehyde

BSA Bovine Serum Albumin

mm Millimeter

nm Nanometer

N Newton

mM Millimolar

ºC Celcius

J Joule

cm Centimeter

W Watt

µg Microgram

mL Milliliter

LIST OF FIGURES

LIST OF TABLES

ÖZET

Doku Mühendisliği Yöntemi İle Elektroeğirilmiş Ön Çapraz Bağ (ÖÇB) İmplantı Hazırlanması

Dünyada ön çapraz bağ (ÖÇB) yırtılmalarının sıklığı aktif yaşam biçimi ve sporun daha da popülerleşmesi ile gittikçe yaygınlaşmaktadır. ÖÇB'nin kendisini iyileştirememesinden ve tedavi edilmemiş bir yırtığın verdiği rahatsızlıkla birlikte sporcular için erken emeklilik anlamına gelmesinden dolayı, hastalar ameliyat olmaya yönlendirilir. ÖÇB yırtılmaları için tedavi altın standardı ÖÇB rekonstrüksiyon ameliyatıdır. Bu ameliyat sırasında yırtık ligament parçaları temizlenir, kemiklere açılmış olan deliklerden hastanın tendonundan hazırlanmış greft geçirilir. Çoğu hasta için rekonstrüksiyon ameliyatı sorunsuz olarak aktif bir hayata geri dönmeyi sağlasa da, bazı hastalar greftin alındığı donör bölgede sorun yaşamaktadır. Kadavralardan alınan greftler, enfeksiyon hastalıkların bulaş riski ve sterilize edilme sürecinin bu greftlerin mekanik özelliklerini etkilemesinden dolayı iyi bir alternatif değildir. Bu sebeple, alınan tendon greftler yerine kullanılmak üzere bir greftin geliştirilmesi için araştırmalar devam etmektedir. Piyasada yapay malzemelerden üretilmiş greftler bulunmaktadır ve bunlar 10 yılı aşkın bir süredir kullanılmaktadır. Ancak doku büyümesinin olmaması ve mekanik yorulma yüzünden greftin başarısız olması sebebi ile cerrahlar tarafından tercih edilmemektedirler. Yapılan bu çalışmada, doku mühendisliği yöntemi ile bir ÖÇB ligament implantının geliştirmesi amaçlanmıştır. Bu nedenle, elektroeğirilmiş ipek fibroin-kolajen tip I fiber matının ve L929 fibroblast hücre yüklü GelMA hidrojelinin bir araya getirilerek oluşan iki katlı yapının kıvrılmasıyla tübüler bir yapı hazırlanmıştır. Canlı-Ölü hücre canlılığı analizi ve Alamar mavisi testinin sonuçları bu tübüler yapının içindeki hücrelerin çoğalabildiğini göstermiştir.

Anahtar Sözcükler: Ön çapraz bağ, doku mühendisliği, elektroeğirme

ABSTRACT

Preparation of a Tissue Engineered Anterior Cruciate Ligament (ACL) by Electrospinning

The incidence of anterior cruciate ligament (ACL) tears is becoming more common around the world as active life style and sports are becoming more popular. As ACL is incapable of healing itself and an untreated tear can lead to severe discomfort along with an early retirement from sports for athletes, patients are encouraged to go through surgery. The golden standard treatment for ACL tears is ACL reconstruction surgery during which the torn ligament stumps are shaved off and a graft prepared from the tendon of the patient is passed through the holes drilled into the bones. While for most patients the reconstruction surgery allows them to return back to an active life without any problems, some patients suffer from the complications on the donor site where the graft was harvested from. As grafts from cadavers have the risk of transmitting infectious diseases and the process for sterilization causes loss of their mechanical properties, they are not a good alternative. Due to this, there is continuous research to develop a graft that could be used instead of harvested tendon grafts. On the market, there are grafts made from synthetic materials and they have been on the use for more than a decade but the lack of tissue regrowth and graft failure due to mechanical exhaustion they are not preferred by surgeons. In our study, the aim was to develop a tissue engineered ACL ligament. This construct was prepared by combining a silk fibroin-collagen type I electrospun fiber mat and GelMA hydrogel loaded with L929 fibroblast cells and rolling this bilayered structured into a tubular shape. Live-Dead cell viability assay and Alamar blue assay results showed that cells within the tubular construct were able to proliferate.

Keywords: Anterior Cruciate Ligament, tissue engineering, electrospinning

1 INTRODUCTION

As sports activity rises across the globe, injuries related to them rises significantly, and one of the most common injuries athletes have been suffering from are the anterior cruciate ligament (ACL) tears. On average there are more than 80 000 surgeries for ACL reconstruction in US [1]. The chance of injury to the ACL was found to be nearly three times more in female athletes than males [2]. Due to the need to return to athletic life and to improve on their quality of life, and ACL injuries lead to knee joint pains, many patients who suffer from ACL ruptures undergo a reconstruction operation followed by a post-operative rehabilitation [3].

In general, during a reconstruction operation for the ACL, the ruptured ends of the ligament are removed. Bone tunnels are drilled at both ends of the tibia and femur to allow the graft prepared from tendon tissue to pass through. The grafts may be harvested from tendons such as patellar or hamstring tendon. For most of these operations, autografts harvested from the patient's own tissue are preferred. Autografts are known to cause additional problems to the patient such as infection, donor site morbidity and weakening of the tendon. Allografts, tissues harvested from a cadaver, may be an alternative to reconstruct the ligament of the patient but there is always the risk of disease transmission, the graft losing its original mechanical integrity after sterilization and rejection of the graft by the host [4,5].

To overcome these shortcomings, researchers have been looking into developing artificial grafts for ACL. Tissue engineering is a research area that is the conjunction of different fields such as medicine and engineering which aims to restore, maintain and improve the damaged tissues of a patient. [6] The constructs produced through tissue engineering consists of cells seeded onto a scaffold. The main aim of these constructs is for them to function on a similar level mechanically and biologically with the natural tissue they are designed to imitate.

The aim of this study was to produce a bilayered tissue engineered anterior cruciate ligament construct and to study this construct under *in vitro* conditions. For

this a fibrous mat with aligned fibers were produced through electrospinning as the bottom layer to imitate the natural alignment of the collagen fibers of the natural tissue, over the fibrous mat a layer of cell loaded GelMA hydrogel was stacked on top and then this bilayered construct was rolled to produce a rolled up structure that could be used in future ACL rupture repair applications. The structure was intended to be suturable, and for medical applications would be used together with a medical grade glue for better attachment to ligament stumps and to keep its rolled up shape. During this study, 3D printed tough PLA rings were used to keep the structure in its tubular shape.

2 BACKGROUND

2.1 Anterior Cruciate Ligament (ACL)

The knee (Figure 1) is a complex joint of the human body and it is responsible for the support of most of the body weight and maintaining the stability throughout daily activities. The joint maintains its function and stability through the primary and secondary stabilizers. The primary stabilizers of the knee are the ligaments that make up the joint, the main ligaments that bear this function are the collateral and cruciate ligaments. The two collateral ligaments, medial collateral ligament (MCL) and lateral collateral ligaments (LCL) give stability to the medial and lateral parts of the knee and to prevent the excessive valgus and varus stresses that appear throughout the movement of the joint; meanwhile the two cruciate ligaments, anterior cruciate ligament (ACL) and posterior cruciate ligament (PCL), are responsible for preventing the displacement of the tibia and femur [7, 8].

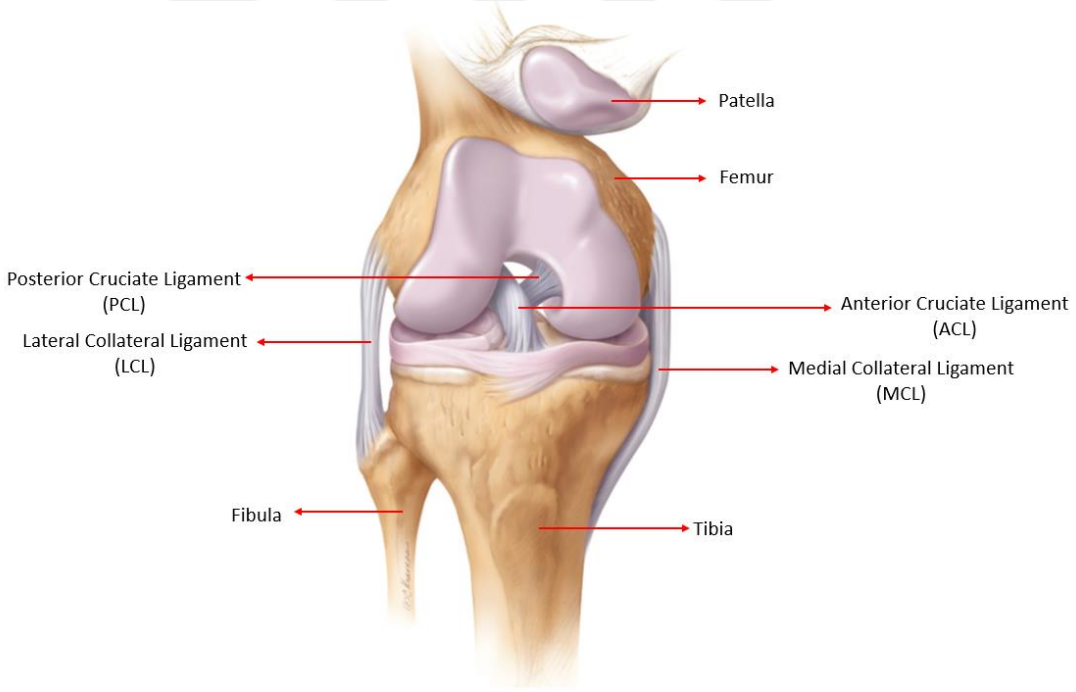

Figure 1 Knee Anatomy. [1]

Focusing on the function of the cruciate ligaments, ACL can be seen performing a double function as it prevents tibia from sliding forward against the femur and it also prevents damage to menisci by maintaining the biomechanical function [9]. ACL is

also considered the main stabilizer of the knee, by taking up more than 80% of the stabilization factor and thus due to this also most commonly ruptured ligament [7]. It is commonly accepted that ACL consists of two main bundles, anteromedial (AM) and posterolateral (PL), and these two bundles work in tandem during the knee's motions. In the extension of the knee, ACL can be more vertically oriented the PL bundle is tighter whereas AM is looser, the opposite is observed for the flexion of the knee [10].

Both bundles are named after their tibial insertions; the AM bundle is at the anteromedial tibial insertion site and PL bundle is at the posterolateral site. When looked at the ACL as a whole it can be seen that it is at its widest at the tibial insertion site, where the fibers of the ligament fan out and form a "foot region", through this ACL wraps itself around the anterior part of the intercondylar notch [11]. For the femoral insertion site, the ligament originates from the medial side of the femoral condyle and from there it runs an oblique course until it reaches tibia [12]. The width and length of the ACL varies, with its width ranging in between 7-12 mm and its length in between 22-41 mm. Surface area of the ACL changes depending on the location, with the smallest surface area of the ACL being its mid-proximal region with 33 mm^2 and the widest being the tibial region with 42 mm^2 [13].

When compared with other ligaments, ACL conforms to the general properties of ligaments such as that it is a white-silvery fibrous structure that connects two bones and is mostly made of collagen. The basic components that make up ligaments can be divided into two, with fibroblasts that secrete collagen and the extracellular matrix (ECM). The ECM is made out of collagen fibrils, water and polysaccharides that trap water. Collagen Type I and Type III abundant in the ligamentous tissue [14]. In ACL, there are two types of patterning that collagen forms; one is a pattern that is sinusoidal, also named as "crimp pattern", and mostly makes up the central part, while the second patterning described as a non-linear/helical wave pattern is called the "recruitment pattern" and makes up the peripheral region. During tensile loading, at low loads crimp pattern straightens out, but as higher loads are applied elongation of the fibrils occur and more of the fibrils, including the recruitment fibrils, are included in the load bearing. These higher loads cause a gradual rise in tissue stiffness, allowing ACL to

protect the knee joint. A collagen fibril has a 25-250 nm diameter, and many fibrils come together to form fibers that form sub-fascicules. A gathering of 3-20 sub-fascicules makes up a fascicle, which has a diameter in the range of 250 μm to several millimeter and along with paratenon they make up the ACL (Figure 2) [13-15].

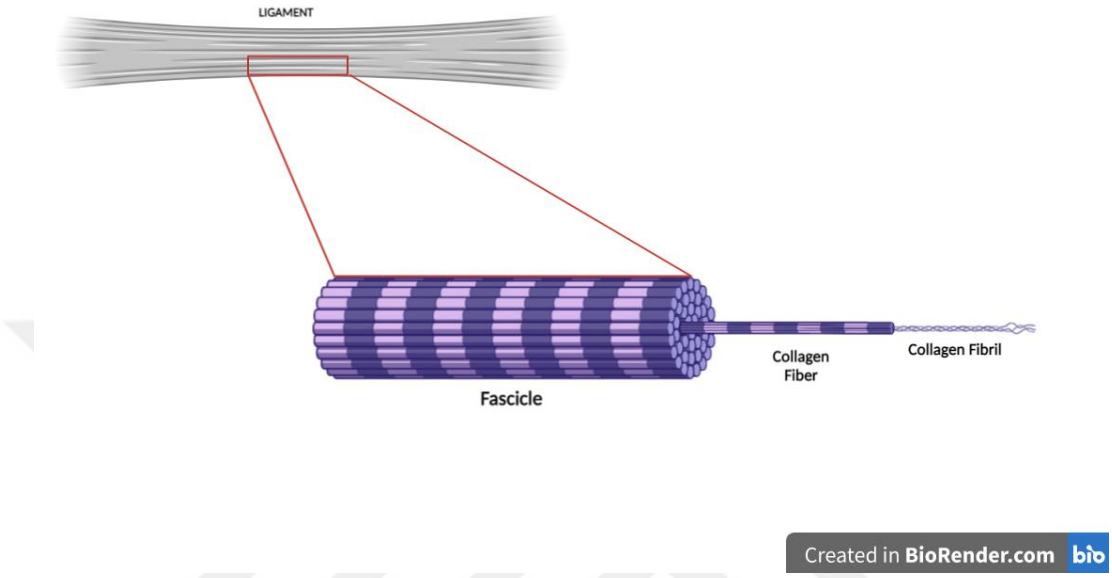

Figure 2 Components of Ligaments.
Created with BioRender.com

Fibroblast cells are lined up in between the collagen fibers, although the properties of the cells change depending on the zonal placement on ACL. There are three main zones along the length of the ligament, named *proximal*, *middle* and *distal* zones (Figure 3). The *proximal zone* is the first one third length from the femoral insertion site of the ACL, is softer and highly cellular when compared to the rest of the structure. The cells in this zone are circular, ovoid cells in addition to the occasional spindle-like fibroblasts. In the *middle zone*, when compared to the other zones there are less cells, they have spindle-like shape and their cytoplasm is closely attached to the collagen fibers to the point of following the crimp pattern. Here, crimp length is higher along with the density of collagen. The distal third of the ligament makes up the *distal zone*. Similar to the *proximal zone*, there is low collagen density and fibroblasts have an ovoid structure. Unlike the other two zones, the bundles of collagen are bigger and the ligament shows fibrocartilage-like properties. The cells have a high activity,

resembling chondrocytes with their ovoid shape and bundling together in rows of groups in between collagen bundles [13, 16].

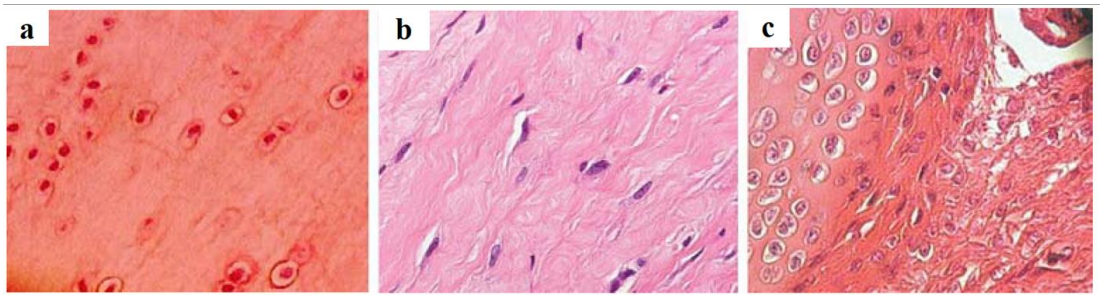

Figure 3 Morphological variation of the cells of ACL depending on their location.
a) Proximal part, ovoid cells; b) Middle part, elongated spindle-like cells; c) Distal part, ovoid cells, with chondrocyte-like properties [13].

While the main blood supply of the ACL is provided by Middle Geniculate Artery (MGA), the synovial sheath that surrounds the ligament allows other blood vessels to enter and follow its path in parallel to the fibrils. The vascularization is present in proximal and middle regions of the ligament but closer to the tibial insertion site. Studies classify the distal region as avascular, while the synovial sheath that covers the ligament is not present in this region [17, 18].

The ACL is innervated through the posterior-anterior branches of the tibial nerve, these nerves penetrate the synovial covering and run along the fascicles. Generally, these nerves have a vasomotor function, with mechanoreceptors having their own responsibilities. There are three types of mechanoreceptors found in the ACL; Ruffini receptors are responsible for sensing the stretching and are generally found near the femoral insertion site, Golgi-like receptors are found near the insertion sites of the ligament and Pacini receptors can be found on the both ends of the ligament and these nerves are responsible to sense compression and rapid movements. The nocireceptors of the ACL are the free nerve endings and they are more numerous compared to the mechanoreceptors. They are responsible for sensing potentially damaging actions to the tissue and have a vasoactive function [19-21].

2.2 Anterior Cruciate Ligament Injuries

When it comes to sports injuries, a study has found that for high school athletes more than half of them were knee injuries and of these ACL injuries made up half of those [2]. In a national population study, it was found that males aged between 20 and 39 who are more active in sports are at a higher risk of an ACL injury [22]. With the rising participation rate of women in sports, studies show that for female athletes the incidence of an ACL injury is higher when compared to a male athlete [2, 23]. When compared with their male counterparts, female athletes had injured their ACL at a more than two times higher incidence rate. The possible causes for this difference could be explained as both external and internal factors. Internal factors for female athletes are based on hormonal, anatomical and neuromuscular functions. There is a debate when it comes to the hormonal factors as researchers cannot reach a consensus. The main point is that the various hormones such as estrogen, progesterone and menstrual cycle based hormones are all changing and in various cyclic stages these hormones may be affecting the biomechanical properties of the ACL. However the data provided by various researchers do not provide a proper evidence [24]. An *in vitro* study on the effect of estrogen and progesterone showed that the change in the concentration of these hormones affect the proliferation rate of human ACL fibroblasts and the synthesis of collagen [25]. These two hormones, depending on the phase of the menstrual cycle have different concentrations. This cycle can be classified into three main phases; the follicular phase (Days 1 through 9) where both progesterone and estrogen levels are low, the ovulatory phase (Days 10 to 14) starts with a surge to the estrogen levels, and during the luteal phase (Days 15 through 28) there is a rise to the progesterone levels [26]. For the clinical findings on the hormonal effects, it was found that the anterior knee laxity was at its lowest at the luteal phase while at the ovulatory phase the anterior knee laxity was at its highest [27]. Anterior knee laxity is a risk factor for ACL injury, and can be defined as "the anterior displacement of the tibia in comparison to femur". Thus, a higher anterior knee laxity poses a higher risk of ACL injury [28]. Another clinical study on female ski athletes found that athletes had a higher incidence rate of ACL injury at late follicular phase [29]. When trying to track the cycle of the athletes along with the incidence of ACL injuries different

methodologies are used to measure hormone levels such as self reporting of the cycle or taking saliva or urine samples. This variation in methodology prevents comparison between studies and a consensus was reached in 2006, which agreed that the currently available studies for the effect the menstrual cycle on ACL are insufficient to come to a conclusion but agreed on the higher injury incidence at both early and late follicular phases [30].

The differences in Q-angle (Table 1) and Notch Width Index (NWI) (Table 2) in between both sexes can be given as anatomical factors for the higher incidence of ACL injuries on female athletes. Q-angle is the angle that is between the line drawn from the anterior superior iliac crest to the center of the patella, and the line drawn from the tibial tuberosity to the same point on patella meanwhile the valgus angle is the angle in-between the femur and the tibia. Both of these angles are prone to change depending on the position of the person and the extension-flexion of the knee but when comparing both sexes, on average females have a higher Q-angle. A high Q-angle means that the valgus angle is high as well. A high valgus angle during movement is known to lead to ACL injury and due to this it is believed that a higher Q-angle increases the risk of an injury [31, 32] due to the mechanism where an increase to the Q-angle, leads to a higher the lateral pull to quadriceps which causes an additional stress to the knee through patella and thus increasing the risk of ACL injury [33].

Table 1 Scheme showing the lines used to calculate Q-angle and factors affecting its calculation [31].

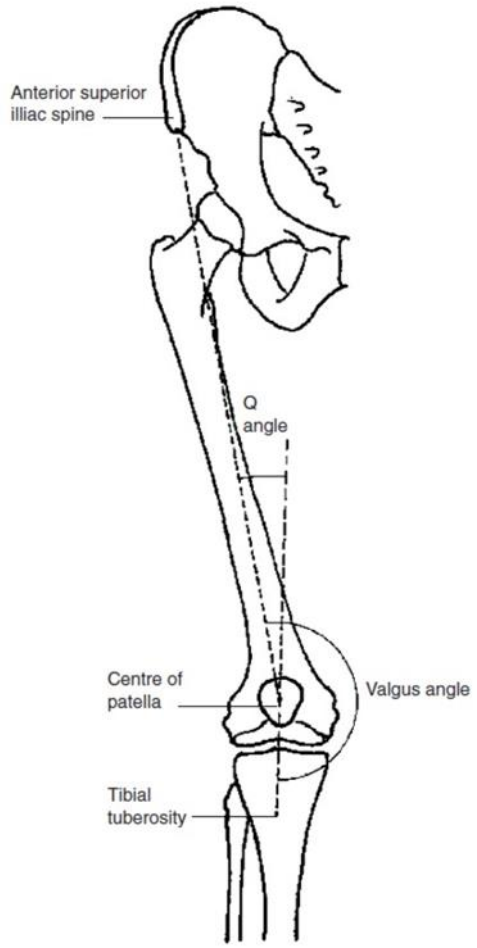	Q-angle is calculated according to the angle in between the vertical line drawn from the center of patella and the line drawn from the center of patella to the anterior superior iliac spine. This angle is affected through anatomical differences such as femur, width of the hips but the stance and the position of the person while the angle is calculated affects the angle as well.

Notch width index (NWI) is the ratio of the intercondylar notch width (INW), the length of the space in between the two tips at the distal end of femur, and the overall length of the distal end of femur. A smaller INW is usually linked to a smaller ACL. For females the INW is smaller when compared to their male counterparts [31]. Having a small INW can cause impingement when the knee is positioned at full extension, a position seen in sports during landing from a jump or during cutting maneuvers [34], both of them common movements where female athletes injure their ACL [35].

Table 2 Scheme showing the lines used to calculate NWI and the factors affecting its calculation [31].

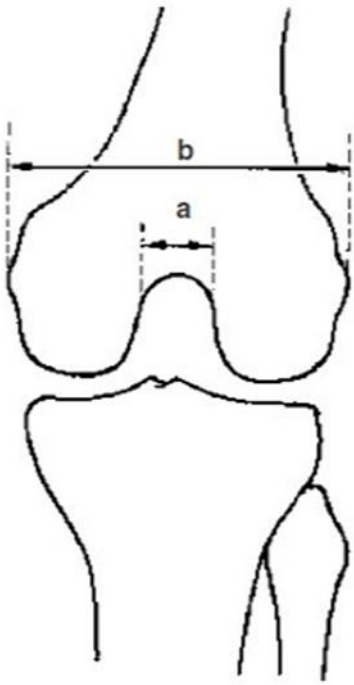	Notch Width Index (NWI) is calculated by the ratio of the intercondylar notch width (INW) (a) to the width of the distal femur (b). While females are associated with having smaller INW thus a smaller NWI, it is also common in men to have a small INW.

At the flexion position, ACL works in tandem with hamstrings to prevent the anterior displacement of the tibia [31], for female athletes' quadriceps has both higher mass and recruitment ratio when compared to hamstring muscles and usually for landing and cutting movements female athletes are shown to be using their quadriceps more. This increases the potential for ACL injury to the increased anterior tibial displacement caused by the contraction of quadriceps muscle [34].

Regardless of gender, for all ACL injuries non-contact injuries make up 70% of them. Meaning that most of the ACL injuries are not caused by a direct force to the knee but by the general movement during sports activities [36]. For a non-contact injury, the athlete has to either to come to a sudden stop or to apply force to the knee from different directions while the foot is bearing weight. An example for the latter situation is when the athlete is landing without regaining their balance properly with their hip turned inwards, they plant their foot to the ground bearing their entire weight onto the lower leg causing forces from opposite sides to be applied to the knee joint

and leading to the ACL to be extended to the point of tearing. Contact injuries requires a direct force to be applied to the knee. These injuries can be caused by the mechanisms similar to that of the non-contact injuries but with contact injuries higher energy is applied and dislocation of the knee, along with damage to other ligaments and structures in the knee joint are possible [37, 38].

ACL injuries are classified according to two factors, the timing of the diagnosis and the size of the tear. For ACL injuries, an acute ACL tear was when the tear was identified within 6 weeks after injury and chronic ACL tear was described as identified at least after 3 to 6 months after injury [39]. Generally complete tears of ACL are easier to clinically diagnose as the tests such as Lachmann test during physical examination give the most accurate results for complete tears while for partial tears physical examination may not give a clear diagnosis and need to be properly diagnosed through Magnetic Resonance Imaging (MRI) or arthroscopy. Of ACL tears, less than 30% can be classified as partial ACL rupture [40.41]. There are different classifications to the partial ACL tears, for both Hong et al. [42] and Noyes et al. [43] classified partial tears according to the amount of fibers that remained untorn, both of them classifying more than 50% intact fibers as partial ACL tear, while according to the classification of the American Medical Association for Athletic Injuries (Table 3) partial tearing of ligaments are classified as 2nd degree sprains as moderate sprains [44]. A general definition of partial ACL tears is when one of the two bundles (PLB or AMB) ruptures while the other bundle remains intact [45]. While it is possible to avoid surgery with partial tears and to have a continued mechanical function patients continue to feel mild to moderate pain and giving way episodes [46], and for young patients who return to an active life generally partial ACL tears progress into complete tears [47].

Table 3 Classification of Sprains by American Medical Association for Athletic Injuries [44].

Classification	Definition
1st Degree Mild Sprain (Minor tear of ligament fibers)	Mild pain, mild tenderness, no abnormal motion, minimal or no swelling, minimal bleeding, minimal loss of function
2nd Degree Moderate Sprain (Partial tear of ligament fibers)	Moderate disability due to pain, slight tenderness, slight-to-moderate abnormal motion, swelling, local bleeding, moderate loss of motion, tendency to recur
3rd Degree Severe Sprain (Complete tear of ligament fibers)	Pain, disability, abnormal motion, possible deformation, tenderness, swelling, bleeding, instability

2.3 Treatment Approaches for ACL

For tendons and ligaments, after a rupture the healing process can be categorized as a normal wound healing process similar to that of the process during skin's healing process, where in time a fibrous structure forms in the place of the wound defect [48, 49]. Of the ligaments, the medial collateral ligament (MCL) is the ligament that has the best understood healing process and it is known to heal without the requirement of surgical intervention. The healing of ligaments can be summarized into three steps: i) early phase also known as the inflammatory phase, ii) proliferative phase and lastly, iii) remodeling phase. The inflammatory phase starts within the first minutes of the tear of the ligament by the start of hemostasis, both of the ruptured ends of the ligament retract themselves and a fibrin blood clot forms. Within the next three to five days, this clot is resorbed and replaced by the cells activated by the inflammatory response. These angiogenic and fibroblastic cells, remove debris from necrotic tissue and start to produce matrix. Following this, in between the gap of the two ends a vascular response causes an increase in both vascularity and blood flow. Around six weeks, proliferative phase starts during which a fibrous scar tissue that connects both ends is formed. In this tissue, collagen type III is much more abundant instead of collagen type I and is more vascular compared to the natural tissue. In time the collagen fibrils,

although their diameters are smaller, become aligned in the direction of the stress. Finally at the remodeling stage, scar tissue loses its cellularity and vascularity in time, and collagen type I becomes more abundant. This healing takes nearly a year and for the ligament may not return to its original performance even after two years [50-52].

For ACL tears, this process is different. The studies [53-55] that follow the progression of ACL tears where patients do not undergo any treatment show that the patients continue to have giving way episodes, with swelling and mild pain and return to sports activity was minimal. A study by Murray et al. [56] has found that due to the intra-articular placement of the ACL does not form a fibrin clotting which is the initial step that allows the cellular proliferation after tear that starts the healing process does not occur, while for MCL is an extra-articular ligament and thus clotting is not impeded. This lack of clotting is caused by the fact that ACL is covered by the synovial tissue, after an injury occurs, the ligament is exposed to synovial fluid which contains hemorrhaging breakdown products and is known to affect ACL fibroblast proliferation in culture negatively [57]. Looking closer at the interaction in between the ACL healing and synovial fluid, Tang et al. [58] discovered that while ACL shows the initial inflammatory phase of the wound healing with the production of the enzymes responsible for the breakdown of collagen debris, the synovial fluid released a much higher amount of these enzymes and disrupting the progression of the healing process.

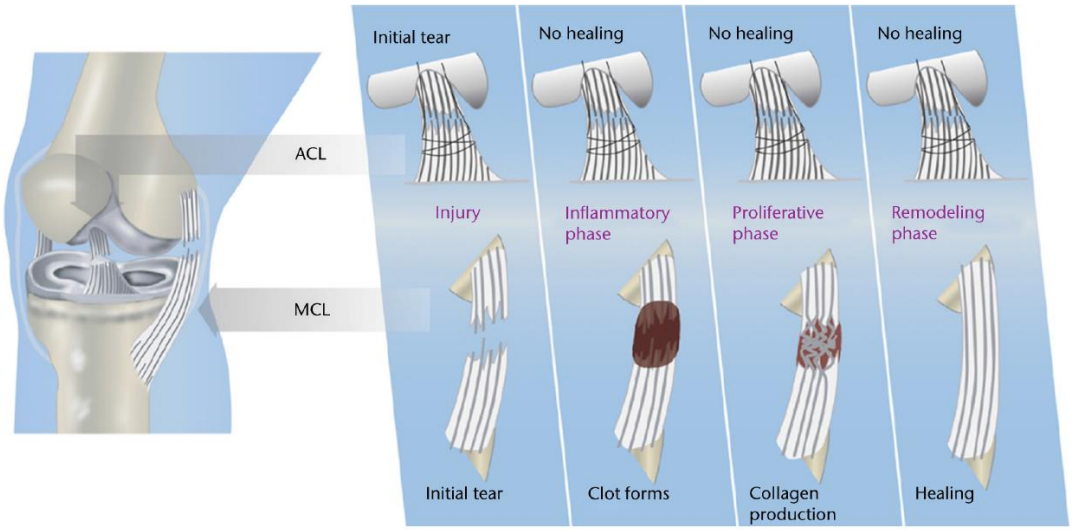

Figure 4 Healing phases of two different ligaments, ACL (at the top) and MCL (at the bottom) [23].

Due to this lack of healing, ACL tears tend to require an operative treatment for the patient to regain normal knee functions. ACL tears are associated with possible damage to menisci and leading to articular cartilage damage, regardless of this some patients may choose not to undergo an operation due to various factors such as age or deciding to quit a life of high-activity [59]. Different considerations are taken into account before starting non-operative treatment, the patient should suffer from an isolated ACL injury, meaning there is no additional injury to the knee and physical therapists employ different tests to measure the patient's suitability for the treatment. Generally, these tests look into knee laxity, knee function, limitation to daily activities and quadriceps strength. After passing these assessments, the patient can be classified as a "coper", a term used clinically that indicates the patient is able to cope with the injury, and allowed to proceed into appropriate physical therapy [60,61]. During physical therapy patient undergoes exercises that aim to help with the reduction in the swelling of the knee, regaining the range of motion of the knee, along with the aim of strengthening of quadriceps and hamstrings to help with joint stability, balance and prevention of anterior translation of tibia. Bracing is also another method for preventing anterior tibial translation [62]. For patients aged 25 and younger, it is suggested that they should undergo an operative treatment instead as non-operative treatment fails for this age group [63].

For a patient who wants to regain pre-injury function of the knee and continue on high activity sports, they have to undergo operational treatment. Currently the gold standard is the ACL reconstruction. During ACL reconstruction, holes are drilled into both femur and tibia, through these holes a graft prepared from harvested tendon tissue is placed and fixed properly. There are many variations that can be considered for this operation. For the holes drilled into the bones, the surgeon may choose to drill a single tunnel or a double tunnel. Single tunnel ACL reconstructions are known for improving the anterior-posterior knee stability but they were lacking when compared to normal knee kinematics. Due to the normal ACL anatomy having two bundles, surgeons are starting to find the double tunnel ACL reconstructions more appropriate as the operations where double tunnel technique was applied results for knee laxity were similar to that of a normal knee but the surgery is harder compared to the single tunnel reconstructions and in the case of improper positioning of bone tunnels the reconstruction surgery would lead to failure [5, 59].

In reconstruction surgeries, the choice for the source of the graft depends on the preference of the surgeon along with the availability of the tissue. Autografts are most commonly used during these operations, because while allografts allow to avoid donor site morbidity the general consensus considers allografts to be mechanically weaker than autografts and the sterilization techniques employed weakens the allografts mechanically. When compared with an autograft of patellar tendon, allograft of the same tissue had a weaker biomechanical property with the allograft having only the half of the tensile load (N) of the autograft [64].

For these surgeries, bone-patellar tendon-bone (BTB) autografts are most commonly used, with 4-string hamstring tendon autografts following second and finally 4-string quadriceps tendon autografts. Quadriceps grafts are more difficult to harvest and literature on its mechanical performance compared to the other two autografts is lacking. When comparing the BTB and hamstring autografts, both grafts seem to have their own advantages and disadvantages (Table 4), with BTB grafts considered as the

more popular option by the surgeons due to its higher strength (nearly three times higher than that of the natural ACL tissue) [4, 64, 65].

Table 4 Advantages and Disadvantages of BTB, Hamstring and Quadriceps Grafts [64, 65].

Graft Types	Advantages	Disadvantages
Bone-patellar tendon-bone	High strength Lower rate of retearing Higher knee stability	Anterior knee pain Higher chance of developing osteoarthritis
Hamstring	Lower chance of donor site morbidity Faster healing	Higher chance of tunnel widening
Quadriceps	Bigger cross-sectional area for grafts Lower chance of pain during kneeling	Difficult to harvest Not enough data in literature

Before reconstruction surgeries became the golden standard, for ACL tears the repair surgery was the preferred method. The technique was first used in 1895, and was properly developed in 1970s-80s into open primary ACL repair. The technique had initially positive results for the patients and had become the standard operation but the mid term follow ups showed that more than 50% of patients suffered from rerupturing of the ligament. With the better results of reconstruction surgeries, ACL repair was abandoned as a technique [66]. In recent years, ACL repair became popularized once more and the possible reasons why the technique did not give out good results was scrutinized. Usage of open arthromies for the surgeries was one of the main criticisms as it caused additional damage to the knee, along with the location of the tear. For tears located on the midsubstance of the ligament, patients required follow up surgeries but for the proximal tears located closer to femoral notch, patients had a much positive outcome [67]. The ACL repair is a technique still in development but it is attractive to many due to it allowing to retain the natural tissue. There is also the possibility of allowing to retain the stumps gives better proprioception, as in the ACL reconstructions where the surgeons decided that there was a chance of reinnervation possibly allowing future regaining of the proprioception of the natural

tissue [5]. As an alternative to auto- and allografts, there are stents, prosthetics and ligament support devices made from various materials available but due to lack of long term results they are not preferrable for clinicians [59].

2.4 Tissue Engineering

Due to risk of donor site morbidity and the potential of the donor tissue losing its previous performance with autografts, and the risk of infection and transmission of diseases from allografts [59], there is a need for an alternative strategy that can overcome these risks for the patient. For this reason, tissue engineering is an attractive area of science for both physicians and researchers alike. The main emergence for tissue engineering is considered to start when in mid 1980s Vacanti and Langer developed a biodegradable scaffold made from synthetic polymers and seeded it with cells, to implant this cell carrying scaffold into animals [68, 69]. Although sometimes both terms of "tissue engineering" and "regenerative medicine" are used interchangeably, tissue engineering is seen as a sub-branch of regenerative medicine where a scaffold is used for tissue regeneration [70]. In their paper titled "Tissue Engineering" Vacanti and Langer defined tissue engineering as "an interdisciplinary field that applies the principles of both engineering and medicine for the development of biological substitutes with the aim of the restoration, maintenance and improvement of the tissue function" [6].

While the main intent for the invention of tissue engineering to develop a structure to support or replace the natural tissue, methods used in tissue engineering can be applied for various purposes. Through *in vitro* models the ethical problem with animal testing can be overcome by using these models for toxicology studies [71], drug development and testing [72] and to understand tissue development and disease modeling [73].

A tissue engineered construct's components can be separated into three main groups (Fig. 4); i) the scaffold that carries and houses the cells, ii) the cells that fill the scaffold, and iii) growth factors that aid in the adhesion, proliferation and/or

proliferation of cells [74]. An ideal scaffold should have the porosity needed for cells to migrate into the scaffold and allow needed nutrients to pass through, while having an absorption rate parallel to that of the healing tissue as scaffolds that degrade slower than the regeneration rate can slow or stump tissue regeneration [70]. Cells in tissue engineering applications are chosen according to the target tissue. While the patient's own cells can preferably be used in culture, there are difficulties in harvesting and these cells can take longer time to proliferate to an appropriate amount. Cells taken from other donor can be utilized but there is still the risk of host rejection and disease transmission. To overcome these, stem cells isolated from different tissues such as bone marrow, adipose tissue, etc. have the potential to differentiate into target cells or cell lines of the target cells can be used in tissue engineering applications [75].

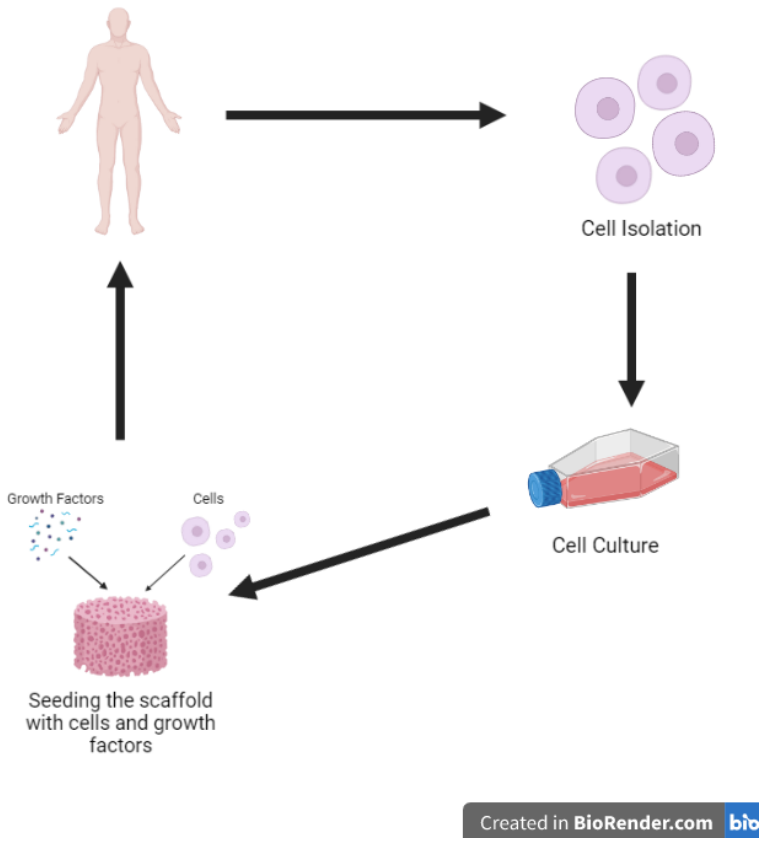

Figure 5 Components of Tissue Engineering.

Created with BioRender.com

2.5 ACL Tissue Engineering

For ACL tissue engineering, it is expected from the construct to be biocompatible and allow cellular and tissue ingrowth, to provide knee stability and biomechanical properties while degrading at a rate that allows transitioning to newly regenerated tissue, and to not require additional surgery [76].

Various materials are used as scaffolds in tissue engineering. These materials can be divided into three categories; synthetic materials, natural materials and decellularized matrices. Synthetic materials have the advantage of being able to be produced in bulk and having controllable mechanical and degradation properties but it is more difficult for cells to adhere to these materials. Natural materials and decellularized matrices are attractive to cells but they have poor mechanical properties and can degrade at a faster rate [77].

Both non-degradable and degradable synthetic materials have been used for ACL tissue engineering. There are grafts for ACL made from non-degrading synthetic polymers available on the market and they are generally made from poly(ethylene terephtalate) (PET), poly(tetrafluoroethylene) (PTFE) and polypyrene. PET, commercially known as Dacron is a strong polymer with high yield strength. A PET graft on the market Ligament Advanced Reinforcement System (LARS), has good initial results but there is a risk of mechanical failure in the long-term due the material deforming under sustained loading [78, 79]. While PTFE as a material has strong mechanical properties, Gore-Tex graft made from braided PTFE showed that the grafts suffered from material fatigue and lack of tissue ingrowth [78, 80]. Polypyrene is another polymer with high mechanical properties and biocompatibility. The Kennedy Ligament Augmentation Device (LAD) that is made from woven braids of polypyrene was intended to give support to weakened tendons and to be used in repair of partial tears of ACL but with the repair surgeries falling out of standard, the high complication rate LADs had in reconstruction surgeries and the retardation in maturation due to stress shielding caused LADs to become obsolete [76, 78]. Other than the grafts that are on the market, different synthetic material applications as scaffolds are being

studied by researchers. The biodegradable synthetic polymers such as poly(lactic acid) (PLA) and poly(glycolic acid) (PGA) are considered gold standard for tissue engineering [75], and there are studies on the application of similar materials such as poly(ε-caprolactone) (PCL), etc. for ACL tissue engineering with various results (Table 5).

Table 5 Studies on ACL tissue engineering using different synthetic materials

Material	Fabrication	Study/Outcome	References
PCL	PCL fibers were bundled together, and then these bundles were grafted with poly(sodium styrene sulfonate).	*in vitro*, with ACL cells isolated from sheep The bundles showed good biomechanical properties even after grafting treatment and cells showed better proliferation and adhesion with grafted bundles compared to the untreated PCL fiber bundles.	[81]
PCL	A PCL fiber mat was prepared through electrospinning and was coated with collagen, plasma etching was used to increase porosity of the fiber mat. Six of these mats were stacked together to produce a scaffold.	*in vivo* (rat), while there was an initial host reaction as the study progressed this response dwindled and collagen deposition increased in time.	[82]
PLA-Poloxamer	PLA-Poloxamer copolymer was spun to produce yarn, with these different scaffolds were prepared through knitting, braiding and rolled knitting.	*in vitro*, with ACL cells isolated from rat PLA-Poloxamer copolymer did not affect cell viability and cellular activity. Of all the various scaffolds, ones prepared through rolled knitting had the mechanical properties most similar to ACL.	[83]

Polymers derived from natural sources are another alternative to develop a tissue engineered ligament as they are more attractive for cells to adhere to [77]. One example of these materials is collagen, found abundantly in natural tissues such as various as bone to cornea and also responsible for the maintenance of both biological and structural integrity of the ECM [84]. There are total of 28 different collagen types identified, and all collagen types share the right handed triple helix shape made from chains that are composed through the repetitions of peptides of glycine-X-Y, where X and Y are usually proline and hydroxyproline. These collagens can be differentiated through their length, the composition of their chains, along with their functions and distribution in tissue. Another method of classification for collagen types is through the supramolecular structures they form, such as fibril forming and network forming, along with other formations. The most commonly found collagens are fibril forming, making up the 90% of the total collagen amount in the body. The fibril forming collagens are the types I, II, III, V and XI, and are mostly found in bone, cartilage, skin and connective tissues. Type II collagen is primarily present in cartilaginous tissues, functioning as a shock absorber and maintaining the tensile integrity of the tissue while type V is associated with types I and III, and can be found around the perimeter of the cells to essentially function as a cytoskeleton. Type III gives the skin its flexibility and is produced at the beginning of the wound healing process. Type I collagen is the most abundant collagen in the body with few exceptions, such as with brain, hyaline cartilage and the vitreous body of the eye. For type I collagen the triple helix formation is constituted of a heterotrimer with two identical α1(I)-chains and one α2(I)-chain coiling around each other. This strand is usually around 300 nm long and through lining up and forming stacks with repetitive 67 nm spacing (D-period), they form collagen fibrils (Figure 6) [85, 86].

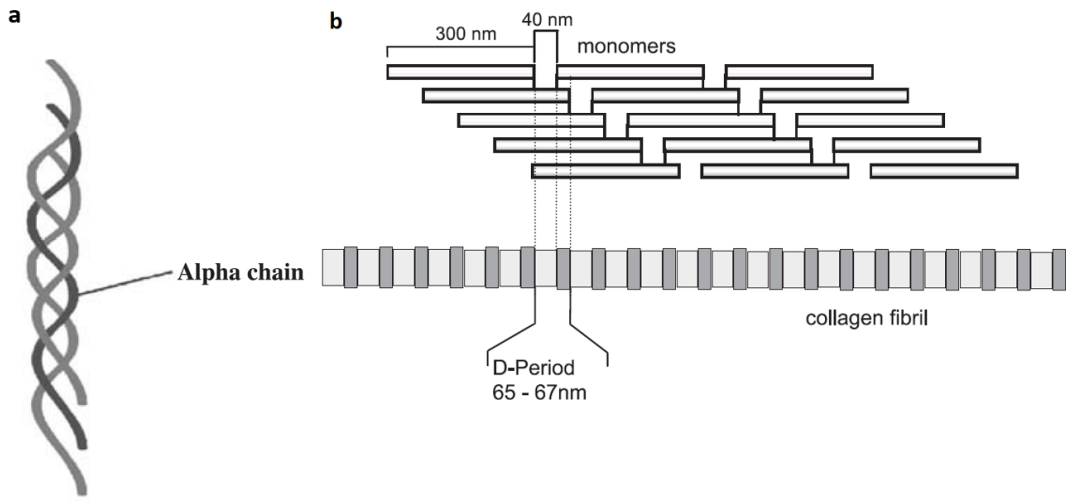

Figure 6 The collagen structure. a) The triple helix formation of alpha chains, b) Formation of collagen fibrils through the characteristic pattern of collagen type I [85,86].

Use of collagen type I as a scaffold material for ligament tissue engineering is common due to its high presence in the native tissue, and there have been previous studies [87, 88] for the implementation of it as a graft but it was found that collagen on its own is weak mechanically and requires crosslinking but this step causes cytotoxic residue and even then the collagen's mechanical performance does not improve [89].

Another commonly used natural polymer used in ligament tissue engineering is silk fibroin due to its unique mechanical properties, such as its tensile strength and toughness [89]. Silk, specifically silk obtained from the cocoons of *Bombyx mori* silkworms has been in use in biomedical applications for a long time as a material for sutures. In nature, a silk fiber is made up of two fibrous proteins weighting 25 and 325 kDa that are covered in sericin, a protein that binds these two proteins together to form the fiber. It has been shown that the presence of sericin affects the biocompatibility of silk, causing an adverse reaction in the host and must to be removed through a degumming process (Figure 7). The silk fibroin proteins, similarly to collagens has a repetitive primary structure that tends to form homogenous secondary structure in

β-sheet form, along with crystals due to hydrogen bonds and hydrophobic interactions. This mixture of β-sheet and crystallinity gives silk fibroin its mechanical properties, with the β-sheet formation affecting the mechanical properties and degradation rate of the material. Through methanol treatment, it is possible to induce crosslinking to transform the random coils to β-sheet structure [90-92].

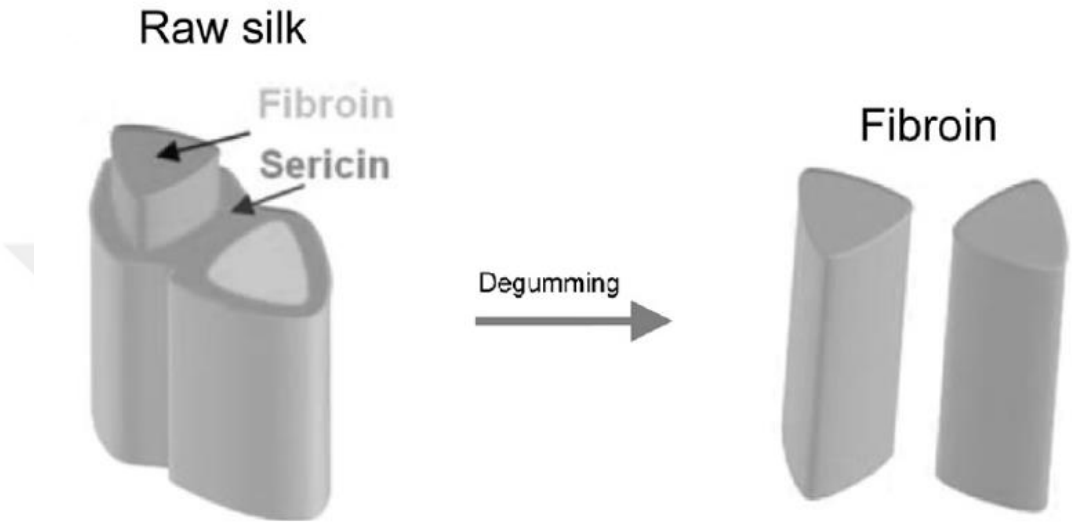

Figure 7 The schematic representation of silk fibroin isolation [91].

For ligament tissue engineering, silk fibroin has been used as scaffold usually either in knitted form or in electrospun form. In their study, Seo et al. [93] had prepared a knitted silk fibroin scaffold to compared its properties with a similarly knitted PGA scaffold both *in vitro* and *in vivo*, with the conclusion that while the silk fibroin had better biocompatibility, mechanically it was weaker than PGA. Jin et al. [94] has shown that a fiber mat of silk fibroin obtained through electrospinning allows attachment of bone marrow-derived mesenchymal cells, a commonly used cell type in ACL tissue engineering [95]. By combining silk fibroin and collagen type I, Maghdouri-White et al. [96] produced an electrospun mat with nanofibers that showed proper cellular attachment and proliferation, with cellular alignment with the fibers.

The fabrication of scaffolds through electrospinning allows for the preparation of scaffolds with fiber diameters on a micro- or nano-scale with alignment that closely

mimics the ligament tissue. At its core, electrospinning is composed of three main parts i) a power supply, ii) a syringe pump and iii) a grounded collector (Figure 8). The syringe pump feeds the dissolved polymer through a needle and the power source is attached to it. The power needed throughout the process is excessive, reaching kilovolts; at a certain value this electrical power reaches the needed to overcome the surface tension of the droplet to form a conical shape called the Taylor's cone and the polymer is ejected as a charged jet. This charged polymer jet is attracted to the grounded collector, as the jet moves towards the collector the solvent of the polymer evaporates and fibers of the polymer are collected on the grounded surface. The alignment of the fibers can be affected depending on the collector used, on a flat surface fibers are collected on a random formation whereas mandrels spun at a certain velocity can be used to obtain aligned fibers [97-99].

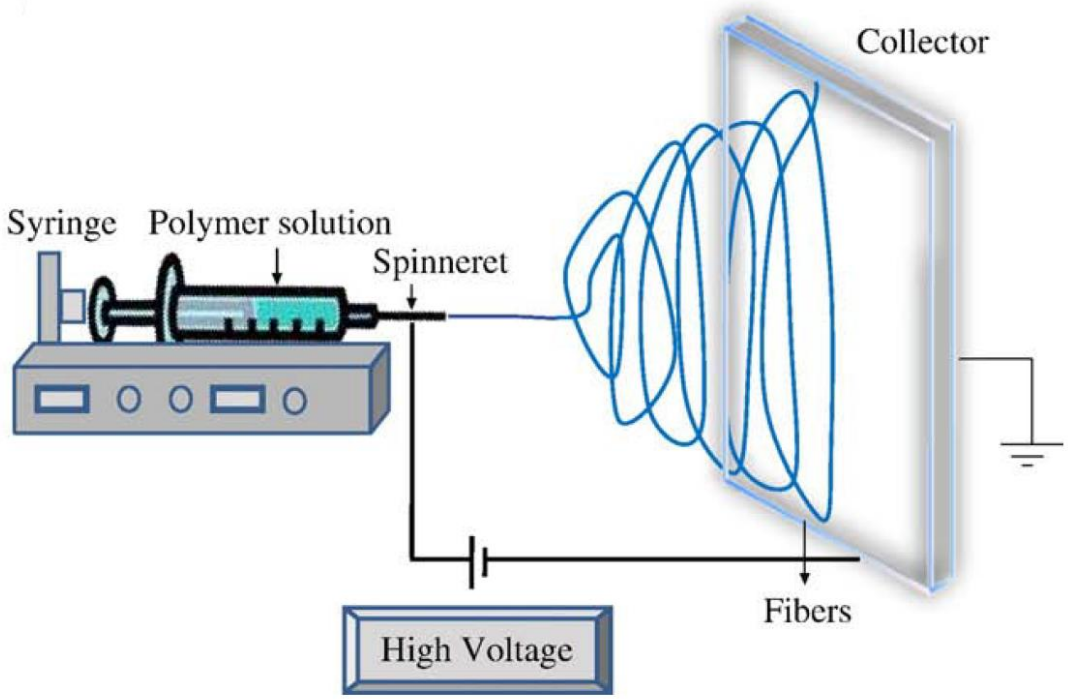

Figure 8 The schematic representation of an electrospinning system [97].

3 MATERIALS AND METHODS

3.1 Materials

Bombyx mori silkworm cocoons were a kind gift from Bursa Metropolitan Municipality (Turkey). Sprague-Dawley rat tails were kindly provided by the Experimental Animals Application and Research Center (DEHAM) of Acibadem Mehmet Ali Aydinlar University (ACU) (Turkey). Sodium carbonate, hydrochloric acid and methanol were purchased from ISOLAB (Germany). Lithium bromide, acetic acid, sodium phosphate monobasic, (1,1,1,3,3,3)-hexafluoro-2-propanol (HFIP), gelatin from porcine skin (300 g bloom), methacrylic anhydride, lithium phenyl-2,4,6-trimethyl benzoylphosphinate (LAP), N,N,N',N'-tetramethyl ethylenediamine (TEMED), ammonium persulfate (APS), trizma base, sodium dodecyl sulfate, and fluorescein isothiocyanate (FITC) conjugated phalloidin were obtained from Sigma-Aldrich (USA). Sodium phosphate dibasic was supplied by AFG Bioscience (USA). DMEM High Glucose medium and 0.25% Trypsin-EDTA were from Gibco (USA). Live/Dead assay kit and Alamar Blue assay kit were purchased from Thermo Fisher Scientific (USA). Fetal Bovine Serum (FBS) was from Biowest (USA). Dimethyl sulfoxide (DMSO) was purchased from WAK-Chemie Medical GmbH (Germany). Coomassie Stain and Laemli Sample Buffer were obtained from Bio-Rad (USA). GenColor Prestained Protein Marker was from GeneMark.

3.2 Methods

3.2.1 Production of ACL Scaffold

3.2.1.1 Isolation of Silk Fibroin from Silk Cocoons

Bombyx mori cocoons were cut and weighed, and then placed in boiling Na_2CO_3 (0.02 M) for 30 min. The threads were dried by placing them in an oven at 37^{o}C overnight. The threads were weighed. LiBr solution (9.3 M) was heated to 60 ^{o}C and was poured over the silk threads. The silk threads were left to dissolve for 4 h at 60 ^{o}C, after which the solution was filtered through filter paper. The filtered solution was

dialyzed (10,000 Da cut-off, Thermo Fisher Scientific) against distilled water for 3 days. The solution was frozen at -80 ºC and were freeze dried (FreeZone Freeze Dry System, Labconco Co., USA).

3.2.1.2 Isolation of Collagen Type I from Rat Tails

Sprague Dawley rat tails, a kind gift from DEHAM, ACU, stored at -80ºC were thawed and their skin was removed, tendons were separated from the tails. The tendons were left to dissolve in cold (4ºC) acetic acid (0.5 M) for 3 days. The solution was then filtered through glass wool to remove non-dissolved connective tissue and the filtered solution was dialyzed (10,000 Da cut-off, Thermo Fisher Scientific) against phosphate buffer solution (at 7.2 pH, sodium phosphate dibasic (12.5 mM), sodium phosphate monobasic (11.5 mM)) for the next 5 days. The solution was removed from dialysis tubes and were centrifuged at 10,000 g for 10 min at 4ºC. The pellets were then dissolved in cold (4ºC) acetic acid (0.15 M) overnight. 5% (w/v) NaCl was added to the solution to precipitate the protein for the next 2 days. The precipitated collagen was collected by centrifuging the solution at 10,000 g for 20 min at 4ºC. The pellets were dissolved in cold (4ºC) acetic acid (0.15 M) overnight, and were then dialyzed against PBS (at 7.2 pH, sodium phosphate dibasic (12.5 mM), sodium phosphate monobasic (11.5 mM)) for the next 5 days. The collagen was then removed from the tubes and was centrifuged at 10,000 g for 20 min at 4ºC. For the next 2 days, the pellets were left to dissolve in 70% ethanol. The solution was then centrifuged at 10 000 g for 30 min at 4ºC. The collagen pellets were then frozen at -80 ºC and were freeze dried (FreeZone Freeze Dry System, Labconco Co., USA). The collagen was kept at 4ºC until further use.

3.2.1.2.1 Analysis of the Isolated Collagen Type I by SDS-PAGE

The purity of the Collagen isolated from rat tails was characterized through sodium dodecyl sulphate-polyacrylamide gel electrophoresis (SDS-PAGE). During electrophoresis proteins are separated according to their masses. SDS is a negatively charged detergent that denatures the proteins into long chains and covers them with a

negative charge, allowing the proteins to be separated according to molecular mass. For additional denaturation, β-mercaptoethanol can be used. Two different gels in different concentrations are prepared, stacking gel that has a lower concentration is used to load the samples and the other gel separates the proteins according to their mass. By applying electrical potential, proteins start to move towards the positively charged electrode.

In this study, separating gel (8%) and stacking gel (4%) solutions were prepared (Table 6), separating gel was poured first into the gel casette and allowed to polymerize at room temperature for 30 min. Afterwards, stacking gel was poured in and the combs were placed in the gel cassette. Two collagen samples (0.02% collagen in 0.02% acetic acid), one of the samples loaded with β-mercaptoethanol, were denatured at 95ºC for 5 min and were then loaded into wells. The applied potential was 180 V and the gel was left to run for 1.5 h. The gel was washed with dH_2O three times and was left in Coomassie Blue overnight to stain the separated protein bands. The next day, the gel was washed in dH_2O for 4-5 h.

Table 6 Separating and Stacking Gel Concentrations.

	Separating Gel (8%)	Stacking Gel (4%)
acrylamide-bisacrylamide (30% stock)	2.66 mL	850 µL
Tris-HCl (1.5 M, pH 8.8)	2.5 mL	-
Tris-HCl (0.5 M, pH 6.8)	-	0.625 mL
10% SDS	100 µL	50 µL
10% APS	100 µL	50 µL
TEMED	5.99 µL	5 µL
dH_2O	4.63 mL	3.4 mL
TOTAL	10 mL	5 mL

3.2.1.3 Production of a Fiber Mat Through Electrospinning

The fiber mat of the outer layer with aligned fibers were obtained through electrospinning. The electrospinning system was composed of power supply (Gamma

High Voltage, USA), syringe pump (New Era Pump Systems Inc., USA) and a rotating mandrel made in our laboratory. The polymer solution was loaded into a syringe with a blunted 26G needle and was pumped through the syringe pump at a constant flow rate. The needle of the syringe is attached to a power supply to create a potential. At a certain potential, this charge changes the formation of the droplet by overcoming the surface tension and a conical shape known as "Taylor's cone" is observed. To achieve this the charge applied to the system needs to be adjusted until the needed voltage value is reached. As the solution is ejected, the charged polymer is attracted to the grounded collector, and as the polymer moves through the air to reach the metal collector the solvent evaporates. To obtain fibers, both the distance between needle and collector and the flow rate needs to be adjusted to a value that produces intended fibers. The concentration of the polymers is another parameter that affects the fiber uniformity, diameter and alignment, to obtain uniform fibers the polymer's ratio both within the solution, and if more than one polymer is used their ratios with each other need to be adjusted. The alignment of the fibers depends on the collector used, a mandrel with a proper rotation speed can be used for obtaining an electrospun mat with aligned fibers. As shown in Table 7, different parameters were used for the optimized values to produce a mat with aligned fibers.

Table 7 Optimization of the Electrospinning Parameters.

Materials	Applied Potential (kV)	Distance (cm)	Flow Rate (mL/h)	Mandrel Speed (rpm)
SF(10%):ColI (10%) (w/v) 1:1	20	16	2.4	725
	20	20	2.4	725
	18	20	2.4	725
	18	20	2.0	725
	18	20	1.8	725
	18	20	1.6	725
	20	20	1.2	725
Silk Fibroin (10% w/v)	18	20	1.2	725
SF (10%):ColI (10%) (w/v) 9:1	18	20	1.2	725
	18	20	1.2	1000
	18	20	1.2	1500
	18	20	1.2	2000
	18	20	1.2	2500
	18	20	1.2	3000

SF:Silk Fibroin, ColI: Collagen Type I

According to the results given in Section 4.2.1, the polymer with optimized concentration was Silk Fibroin (10% w/v):Collagen Type I (10% w/v) at a 9:1 ratio. The polymer was prepared by dissolving both materials separately in HFIP and after that they were mixed. The optimized electrospinning parameters for the system were: 18 kV applied potential, 1.2 mL/h flow rate and 20 cm distance. The mandrel (15 cm in diameter) of the collector was covered with a PEG coated aluminum foil and was rotated at 2500 rpm. The obtained fibers were treated with methanol (99%) for 45 min to set them and removed (Figure 9).

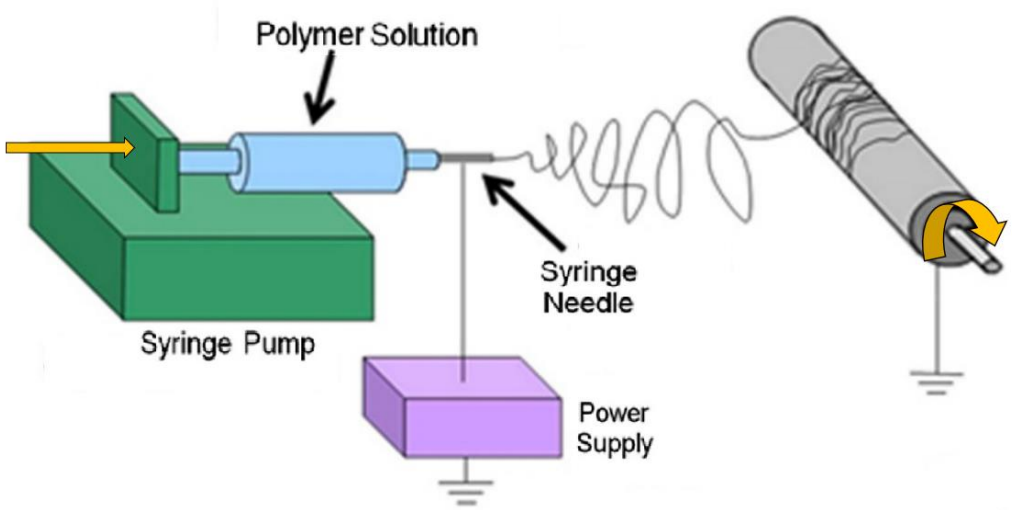

Figure 9 Electrospinning system. [100].

3.2.1.4 Characterization of the Electrospun Mat

3.2.1.4.1 Scanning Electron Microscopy

Morphology of the fiber mats was studied using the Scanning Electron Microscopy (SEM) (EVO 10, Zeiss, Germany). The mats were placed onto aluminum stubs, and coated with gold under vacuum for 2 min (Q150RS, Quorum, UK).

3.2.1.4.2 Mechanical Testing

Tensile testing was done to determine the mechanical properties of the electrospun fiber mats using Mechanical Testing Machine (Shimadzu AGS-X Series Universal Test Machine, Japan) with 5 kN load cell at the speed of 1 mm/min, and Mechanical Testing Software (Trapezium, Shimadzu, Japan).

3.2.2 Synthesis of GelMA

In order to prepare GelMA, initially Dulbecco's phosphate buffered saline (DPBS) (Gibco) (200 mL, 10 mM) was preheated to 60°C and then 20 g of porcine skin gelatin was added. Methacrylic anhydride (13.4 mL) was added to the solution dropwise and the solution was left at 55°C for 2 h. The methacrylation reaction was stopped by adding DPBS (400 mL). The solution was dialyzed (10,000 Da cut-off, Thermo Fisher Scientific) against dH_2O for 10 days to remove excess methacrylic anhydride. After dialysis, the solution was filtered. Finally, the solutions were lyophilized (FreeZone Freeze Dry System, Labconco Co., USA) and kept at -80°C until further use.

3.2.2.1 Characterization of GelMA

3.2.2.1.1 ^{1}H-Nuclear Magnetic Resonance (^{1}H-NMR) of GelMA

In order to measure the methacrylation degree of the gelatin, both gelatin and dried GelMA were dissolved in D_2O to obtain their ^{1}H NMR spectra, using Bruker Biospin High Resolution Digital 300 MHz NMR Spectrometer (The Central Lab, METU, Ankara). The equation given below was used to calculate the methacrylation degree (MD).

$$\text{MD (\%)} = \left(1 - \frac{\text{Peak area of Lysine Methylene of GelMA}}{\text{Peak area of Lysine Methylene of Gelatin}}\right) \text{x}100$$

MD (%): Methacrylation Degree

3.2.2.1.2 Determination of Equilibrium Water Content (EWC)

GelMA slabs were prepared by dissolving GelMA in DPBS (16% w/v) at 37°C, and lithium phenyl-2,4,6-trimethyl-benzoyl-phosphinate (LAP) 10% (v/v) photoinitiator was added to this solution. The GelMA solution was added into the wells of a 96 well plate and was then exposed to UV (365 nm, 0.6 Joule/cm^2) for 2 min in a UV chamber (BIO-LINKTM BLX, Germany). After removing the slabs from the wells, GelMA slabs were immersed in PBS at 37°C for 24 h. After excess PBS was

removed with a filter paper, the slabs were rinsed with distilled water and their wet weight (W_w) was recorded. The slabs were frozen at -80ºC and then lyophilized to record their dry weight (W_d). Equilibrium water content (EWC) of the GelMA slabs were calculated according to the equation given below:

$$EWC\ (\%) = \frac{W_w - W_d}{W_w}\ x\ 100$$

EWC (%): Equilibrium Water Content (%)

W_w: Wet Weight

W_d: Dry Weight

3.2.2.1.3 Mechanical Testing

Mechanical properties of the GelMA were examined through the compression tests on GelMA slabs using Mechanical Testing Machine (Shimadzu AGS-X Series Universal Test Machine, Japan) at a displacement rate of 0.5 mm/min. GelMA slabs were prepared as in Section 3.2.2.1.2. The results were analyzed using Mechanical Testing Software (Trapezium, Shimadzu, Japan). For each sample, a stress-strain curve was obtained and from the slope of the linear region of this curve the compression modulus of the samples was calculated according to the equations given below:

$$Strain\ (\varepsilon) = \frac{\Delta l}{l}\ \text{(I)}$$

$$Stress\ (\sigma) = \frac{F}{A}\ \text{(II)}$$

$$Compressive\ Modulus = \frac{\sigma}{\varepsilon}\ \text{(III)}$$

Δl: Displacement (mm)

l: Initial length (mm)

F: Applied Force (N)

A: Cross-sectional area of the sample (mm^2)

3.2.3 Construction of the Bilayered of GelMA-Electrospun Fiber Tube

In order to form the GelMA layer of the tubular structure, a mold made from Tough PLA was produced through 3D printing. The mold was designed in SketchUp (Google Inc., USA) and loaded to the Ultimaker Cura 3.5.3 software of the Ultimaker S5 3D printer (Ultimaker, Netherlands) for printing. The GelMA solution was prepared as the Section 3.2.2.1.2 and then transferred into the mold with a micropipette. The molds containing GelMA solution were placed in a UV chamber (BIO-LINKTM BLX, Germany) to expose GelMA to UV (365 nm, 0.6 J/cm^2) for 2 min.

The electrospun fiber mats were cut into squares (2 cm x 2 cm) and treated with oxygen plasma on both sides (50 W for 3 min). After GelMA layer was prepared, the fiber mat was placed on top of it while it was still in the mold. The bilayered product was removed from the mold and exposed to UV for 30 s. The structure was then rolled into a cylinder starting from one corner, and in parallel to the alignment of the fibers (Figure 10).

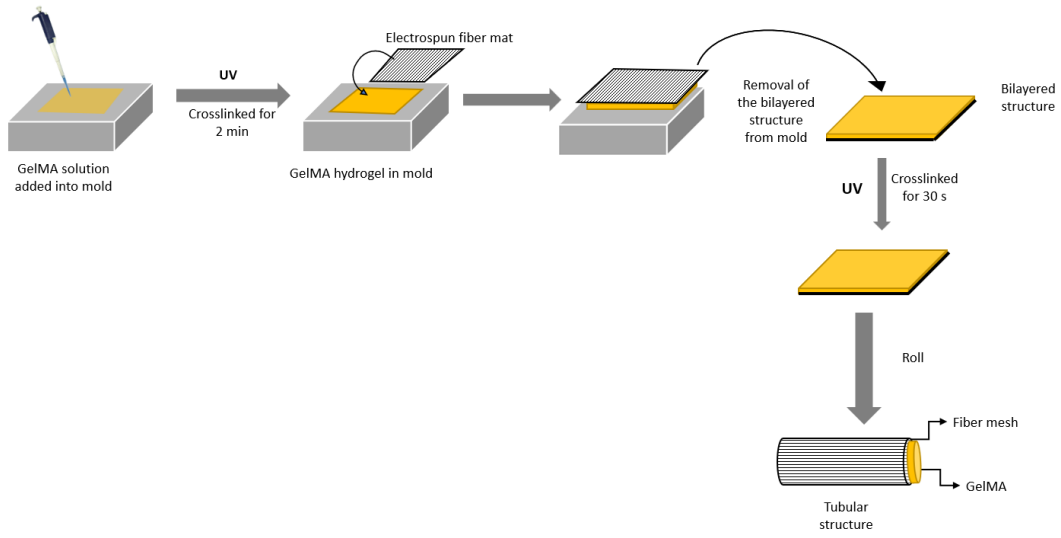

Figure 10 Construction of the bilayered GelMA-Electrospun Fiber tube.

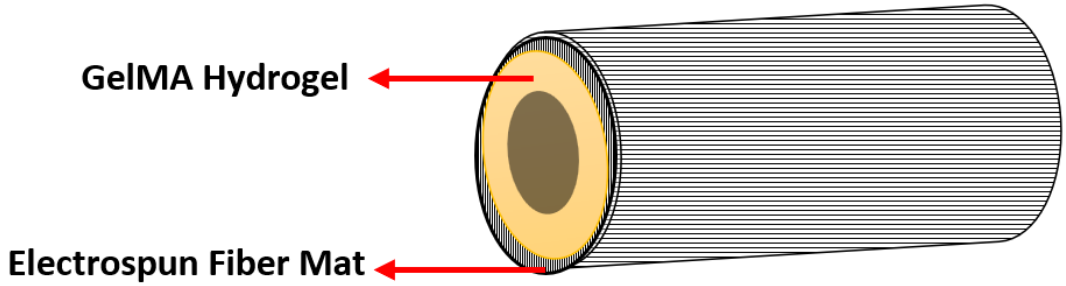

Figure 11 The bilayered tube.

3.2.3.1 Characterization of the Bilayered GelMA-Electrospun Fiber Tubes

3.2.3.1.1 Scanning Electron Microscopy (SEM)

In order to examine the hydrogel layer while it was still moist, the samples were placed under low vacuum using Scanning Electron Microscopy (SEM) (Thermo Quatro ESEM at Acıbadem Mehmet Ali Aydınlar University).

The bilayered tubes were lyophilized (FreeZone Freeze Dry System, Labconco Co., USA) after freezing at -80ºC to prepare them for Scanning Electron Microscopy (SEM) (EVO 10, Zeiss, Germany). The samples were placed onto aluminum stubs, and coated with gold (Q150RS, Quorum, UK).

3.2.4 *In vitro* Studies

L929 fibroblast cell line (ATCC, USA), which was a kind gift from METU BIOMATEN Center in Ankara, TURKEY, was used for *in vitro* studies because fibroblasts are the local cell population found in the native tissue.

3.2.4.1 Culture of L929 Fibroblast Cells

L929 cells in Passage 23 were cultured in a medium containing DMEM High Glucose, 10% FBS and Penicillin (100 U/mL)/Streptomycin (100

μg/mL)/Amphotericin-B (0.25 μg/mL) (P/S/A) in tissue culture polystyrene flasks. Culture media of cells were changed every 2 days.

3.2.4.2 Preparation of Cell Loaded GelMA Slabs

GelMA solution was prepared by dissolving GelMA in culture media at 37°C and then filtering the solution through a 0.22 μm syringe filter in a laminar flow cabin. LAP (10% v/v) was added to the GelMA solution after filtering. The solution was kept at 37°C until further use.

Once cells reached proper confluency (80%) , they were detached from culture flasks by adding 0.025% Trypsin-EDTA, centrifuged at 1500 rpm for 5 min and the resulting pellet was then resuspended in 1 mL of culture medium. Cells were counted using a Thoma (ISOLAB, Germany). The intended amount of cells (10^6 cells) were removed and placed into a separate falcon tube to be centrifuged, the cell pellet was resuspended in GelMA solution. GelMA solution carrying 10^6 cells was added into the wells of a 96 well plate and then crosslinked under UV (365 nm, 0.6 Joule/cm^2) for 2 min in a UV chamber (BIO-LINKTM BLX, Germany). The crosslinked GelMA slabs were placed into the wells of a 24 well plate, enough culture media containing DMEM-High Glucose, 10% FBS and P/S/A was added and cells within the hydrogel were cultured in a CO_2 incubator at 37°C, 5% CO_2. The culture media was changed every 2 days.

3.2.4.3 Live-Dead Cell Viability Assay of GelMA Slabs

After eight days of culture, Live-Dead Cell Viability Assay was conducted to determine the viability of cells in GelMA hydrogel slabs. Assay solution was prepared in DPBS with calcein AM (0.5 μL/mL) for live cells (green) and ethidium homodimer-1 (2 μL/mL) for dead cells (red). After the culture media was removed, Live-Dead assay solution was added into the wells and the samples were incubated at 37°C for 30 min. After incubation, the assay solution was removed, DMEM-High Glucose without Phenol Red was added onto the samples and the samples were examined with Confocal

Laser Scanning Microscopy (CLSM) (Zeiss LSM 900, Germany). The images were examined and the viability of cells were calculated according to the equation given below.

$$Viability\ of\ cells\ (\%) = \frac{Live\ Cells\ (Green)}{Total\ Cells\ (Green+Red)}\ x\ 100$$

3.2.4.4 Construction of Bilayered Cell Loaded GelMA-Electrospun Fiber Tube

The cell loaded GelMA solution was prepared as in the Section 3.2.4.2. In order to prepare the cell loaded GelMA layer, the molds sterilized with 70% EtOH for 1 h and exposed to UV light under laminar flow for 1 h for both sides were used. SF-Col1 fiber mats were treated with O_2 plasma on both sides (50 W for 3 min), and then with UV for 1 h on both sides under laminar flow.

After the cells were suspended in GelMA solution, it was poured into the molds and were crosslinked with UV (365 nm, 0.6 Joule/cm^2) for 2 min. The fiber mat was placed onto the slab and the bilayered structure was transferred to a 6 well plate. The bilayered structure was exposed to additional UV for 30 s. The structure was then rolled and then two rings were placed at 2 ends to prevent uncoiling during culture. Enough culture medium containing DMEM-HG, FBS and P/S/A was put into the wells to fully submerge the construct. Media was changed every two days.

3.2.4.5 Cell Behavior in the Tubular Construct

3.2.4.5.1 Cell Proliferation on the Tubular Construct: Alamar Blue Assay

Alamar Blue Assay is a method that measures the metabolic activity of cells, where the cells reduce the blue colored, non-fluorescent resazurin to the purple-pink, highly fluorescent resofurin as shown in the reaction below. By measuring the fluorescence of the resulting solutions, the viability of the cells can be calculated from a calibration curve.

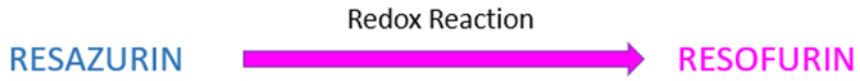

Alamar Blue solution (10% v/v) was prepared with DMEM-High Glucose without Phenol Red and P/S/A. Readings were made on Days 1, 3, 7 and 14. After the media was removed from the wells with samples (n=3), they were washed twice with PBS (with Ca^{2+}, Mg^{2+}). Alamar Blue solution was added into wells, and the well plate was covered with aluminum foil. The samples incubated for 1 h at 37°C in a CO_2 incubator. After incubation, the solutions were divided into the wells of a 96 well plate (10 wells/sample and five wells were filled with Alamar Blue Solution as blank). An Absorbance-Fluorescence Plate Reader (Perkin Elmer, USA) was used to measure the absorbance of the products. Two measurements at 570 nm and 600 nm were made. The reduction in the absorbance of the product was calculated according to the equation given below.

$$\text{Reduced (\%)} = \frac{((\varepsilon_{ox})_{\lambda_2} \times A_{\lambda_1}) - ((\varepsilon_{ox})_{\lambda 1} \times A_{\lambda 2})}{((\varepsilon_{red})_{\lambda 1} \times A'_{\lambda 2}) - ((\varepsilon_{red})_{\lambda 2} \times A'_{\lambda 1})} x100$$

λ_1= 570 nm λ_2= 600 nm

$(\varepsilon_{ox})_{\lambda 2}$ = 117.216 $(\varepsilon_{red})_{\lambda 1}$ = 155.677

$(\varepsilon_{ox})_{\lambda 1}$ = 80.586 $(\varepsilon_{red})_{\lambda 2}$ = 14.652

$A_{\lambda 1}$= Test well at λ_1

$A_{\lambda 2}$= test well at λ_2

$A'_{\lambda 1}$= Blank at λ_1

$A'_{\lambda 2}$= Blank at λ_2

ε_{ox}: Excitation coefficient of the oxidized state of the molecule

ε_{red}: Excitation coefficient of the reduced state of the molecule

3.2.4.5.2 Live-Dead Cell Viability Assay of the Tubular Construct

Live-Dead Assay solution was prepared as same in the Section 3.2.4.3 and the same procedure was applied to the samples (n=2). The assays were performed for Days 3 and 14. The images were obtained with CLSM (Zeiss LSM 900, Germany). The viability of cells was calculated using ImageJ NIH software with the same equation in Section 3.2.4.3.

3.2.4.5.3 Cell Morphology on the Tubular Construct: Phalloidin-DAPI Staining

In order to examine the morphology of the cells within the tubular constructs, the cells were stained with FITC conjugated Phalloidin and 4', 6-diamidino-2-phenylindole (DAPI). Phalloidin stains the actin filaments of the cells while DAPI stains the nucleus. The samples were fixed on Days 3 and 7 with 4% PFA at room temperature, and then washed with PBS. The cells were permeabilized with 0.1% Triton X-100 for 5 min at room temperature. After washing with PBS, the samples were kept in 1% BSA for 30 min at 37^{o}C. The samples were first stained with Phalloidin (1:100 in 0.1% BSA) and were then counterstained with DAPI (1:5000, in PBS). The cells were examined and their images were obtained with CLSM (Zeiss LSM 900, Germany).

4 RESULTS

4.1 SDS-PAGE Results of the Isolated Collagen Type I

The result of the gel electrophoresis for the Collagen Type I isolated from rat tails is shown below (Figure 12). The first lane had the protein marker, and the remaining lanes were loaded with the isolated collagen. In the last lane, the collagen sample was loaded with mercaptoethanol for additional denaturing to obtain clearer lanes. Collagen Type I shows doublets at 115 and 130 kDa and 215 and 235 kDa. Both of the samples had bands at the indicated molecular weights of 115 and 130 kDa, meaning that the protein isolated from rat tails were Collagen Type I.

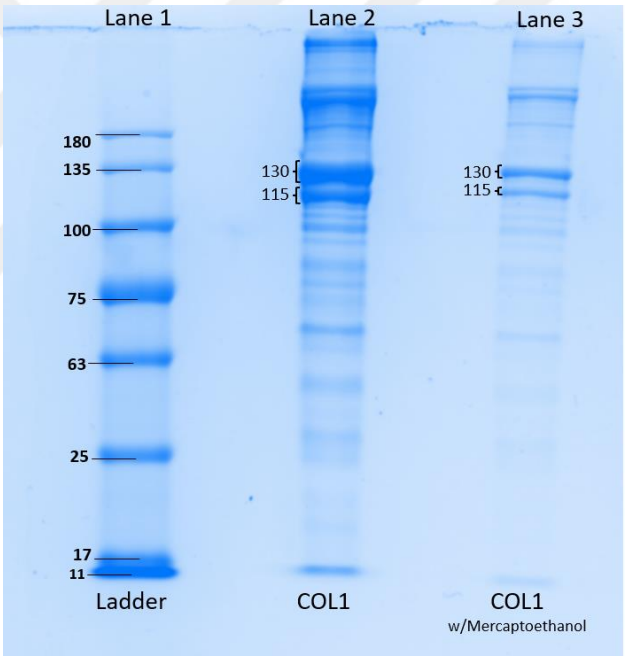

Figure 12 SDS-PAGE of Type I collagen isolated from rat tail; Lane 1: Protein Ladder, Lane 2: isolated collagen type I sample (0.2% w/v) and Lane 3: isolated collagen type I with mercaptoethanol (0.2% (w/v)).

4.2 Characterization of the Electrospun Fiber Mat

4.2.1 Optimization of the Electrospinning Parameters

The natural ACL tissue is composed of bundles of aligned fibrils, with Type I collagen being the most abundant [14]. The aim of the present study was to imitate this organization by producing a fiber mat with aligned fibers by electrospinning. The parameters of the electrospinning system such as the potential, flow rate, distance between the needle tip and the collector, polymer concentration and rotation speed of the mandrel collector was changed until the optimal parameter values for the production of aligned fibers were found. In the first run, the parameters were as presented in Table 8. The fibers of the resulting mat were fused, the fibers were not fully separated from each other (Figure 13a). In electrospinning Run II, while the applied voltage, flow rate and mandrel speed remained constant, distance was increased from 18 cm to 20 cm. The fibers of this mat also had fusion (Figure 13b).

Table 8 Parameters of the Electrospinning Runs I-VII

Electrospinning Run	Materials	Potential (kV)	Flow Rate (mL/h)	Distance (cm)	Mandrel Speed (rpm)	Comments
I	SF (10%):ColI(10 %) (w/v) 1:1	20	2.4	16	725	Fused fibers
II				20		Fused fibers
III		18				Fused fibers
IV			2.0			Fused fibers, with slight uniformity
V			1.8			Fused fibers, with higher uniformity
VI			1.6			Fused fibers, with higher uniformity
VII		20	1.2			Fused fibers, with higher uniformity

SF: Silk Fibroin, ColI: Collagen Type I

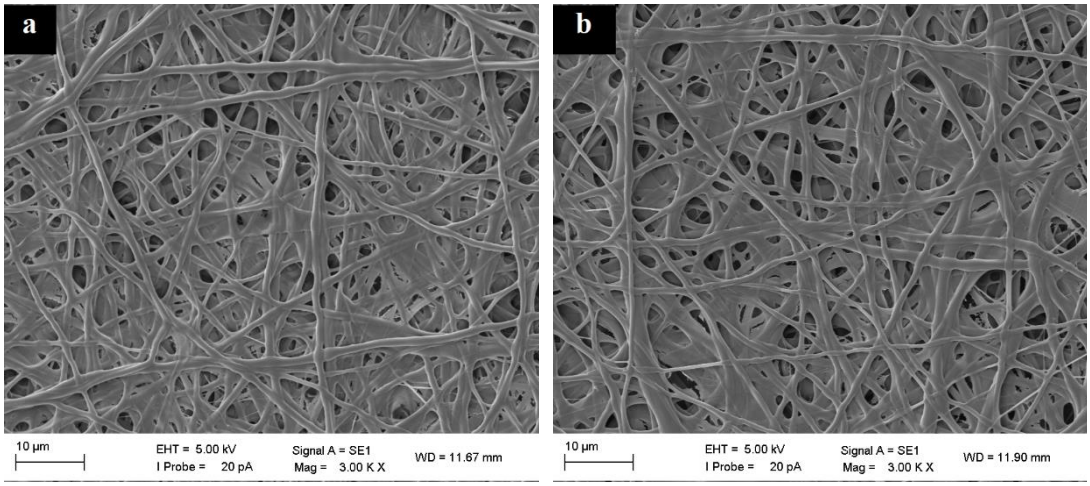

Figure 13 SEM images of electrospun fibrous mats obtained by electrospinning. (a) Run I and (b) Run II. Magnification x3000; scale bar 10 µm.

Then for the next Runs (III-VI), the applied potential was decreased to 18 kV, while the distance and mandrel speed remained the same and four different fiber mats were produced with these parameters. The fibers produced at Run III (Figure 14a) and at Run IV (Figure 14b), had fusion, while there was an improvement on uniformity of the fibers at Run V (Figure 14c) and Run VI (Figure 14d). Out of all four of these mats, the fibers produced with 1.6 mL/h presented the lowest fusion.

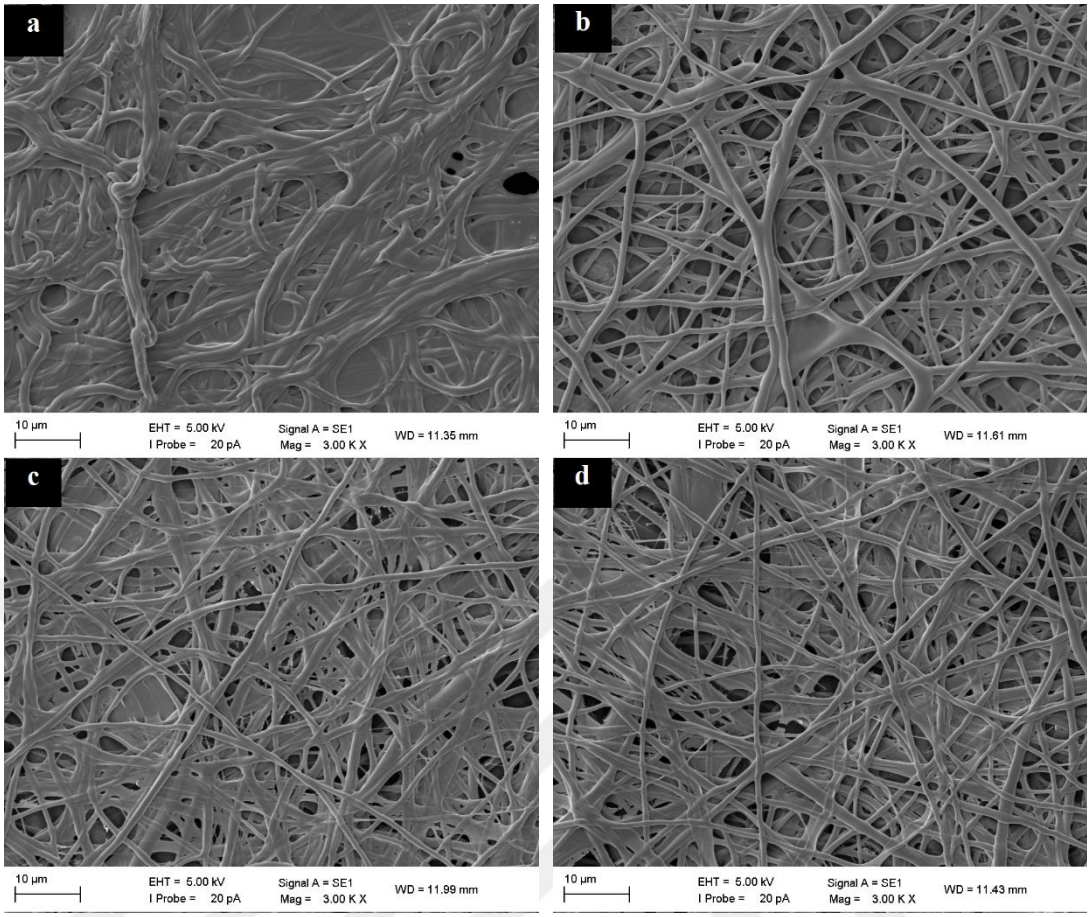

Figure 14 SEM images of electrospun fibrous mats obtained by electrospinning. (a) Run III; (b) Run IV; (c) Run V and (d) Run IV. Magnification x3000; scale bar 10 µm.

Seeing as lowering the flow rate gave better uniform fiber formation, in the next run (Run VII) flow rate was lowered to 1.2 mL/h. The fibers of this mat (Figure 15), also presented fusion.

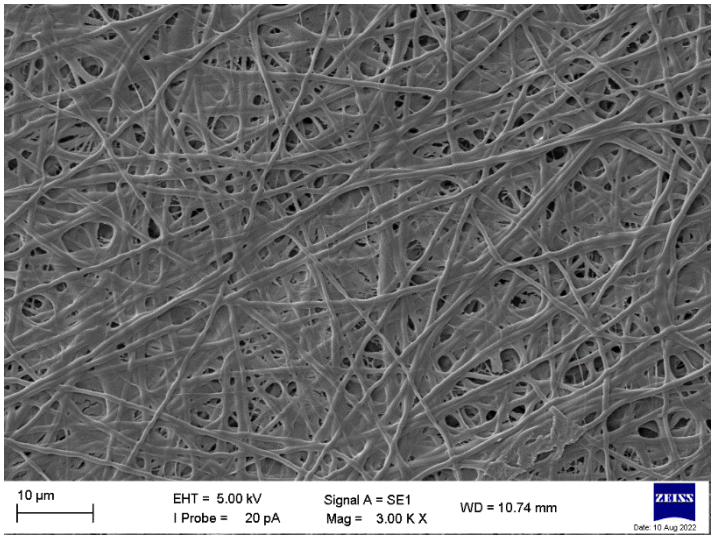

Figure 15 SEM image of electrospun fibrous mat obtained by electrospinning, Run VII. Magnification x3000; scale bar 10 µm.

As the fusion of the fibers could not be fully solved by changing the parameters of the electrospinning system the 1:1 ratio of the two polymer materials was changed to only Silk Fibroin (10% (w/v)) (Run VIII). The resulting mat (Figure 16) had uniform fibers as was intended, although the fibers not organized.

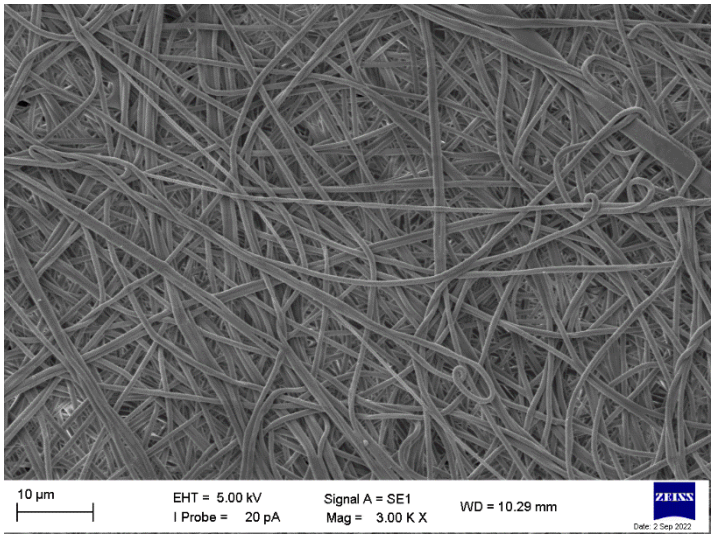

Figure 16 SEM image of electrospun fibrous mat obtained by electrospinning, Run VIII. Magnification x3000; scale bar 10 µm.

As seen in the absence of fusion of the fibers upon use of only Silk Fibroin, the ratio of Col1 was decreased in the blend. Due to this, for Run IX the parameters shown

in Table 9 were applied. As predicted, the fibers produced were uniform and not fused, randomly distributed (Figure 17).

Table 9 Parameters of the Electrospinning Runs IX-XIV

Electrospinning Run	Materials	Potential (kV)	Flow Rate (mL/h)	Distance (cm)	Mandrel Speed (rpm)	Comments
IX	SF(10%);ColI(10%) (w/v) 9:1	18	1.2	20	725	Uniform fibers, with random organization
X					1000	Uniform fibers, with random organization
XI					1500	Uniform fibers, with random organization
XII					2000	Uniform fibers, with mostly aligned organization
XIII					3000	Fused fibers, with aligned organization
XIV					2500	Uniform fibers, with aligned organization

SF:Silk Fibroin, ColI: Collagen Type I

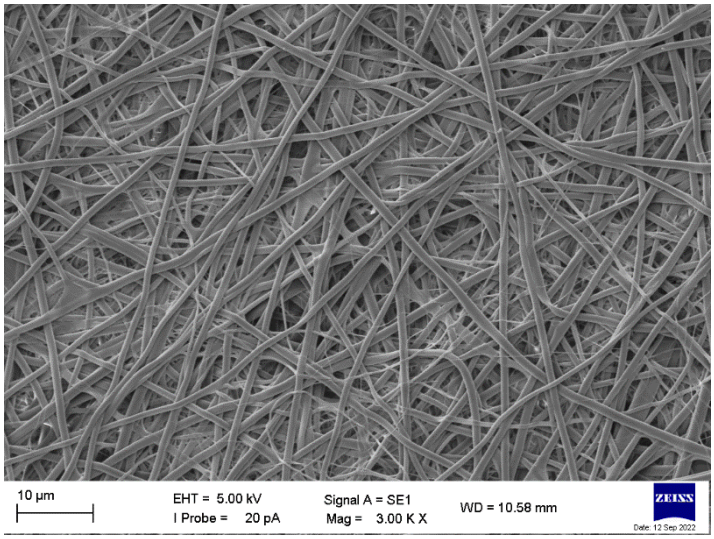

Figure 17 SEM image of electrospun fibrous mat obtained by electrospinning, Run IX. Magnification x3000; scale bar 10 µm.

As fusion of the fibers were decreased to an acceptable degree, mandrel speed was optimized to obtain aligned fibers. In the following Runs (X-XII), the mandrel speed was increased. The fibers of the mats produced at Run X (Figure 18a) and Run XI (Figure 18b) showed random fiber formation, while for Run XII (Figure 18c) fibers started to show some alignment and at Run XIII (Figure 18d) the fibers were aligned although they started to fuse.

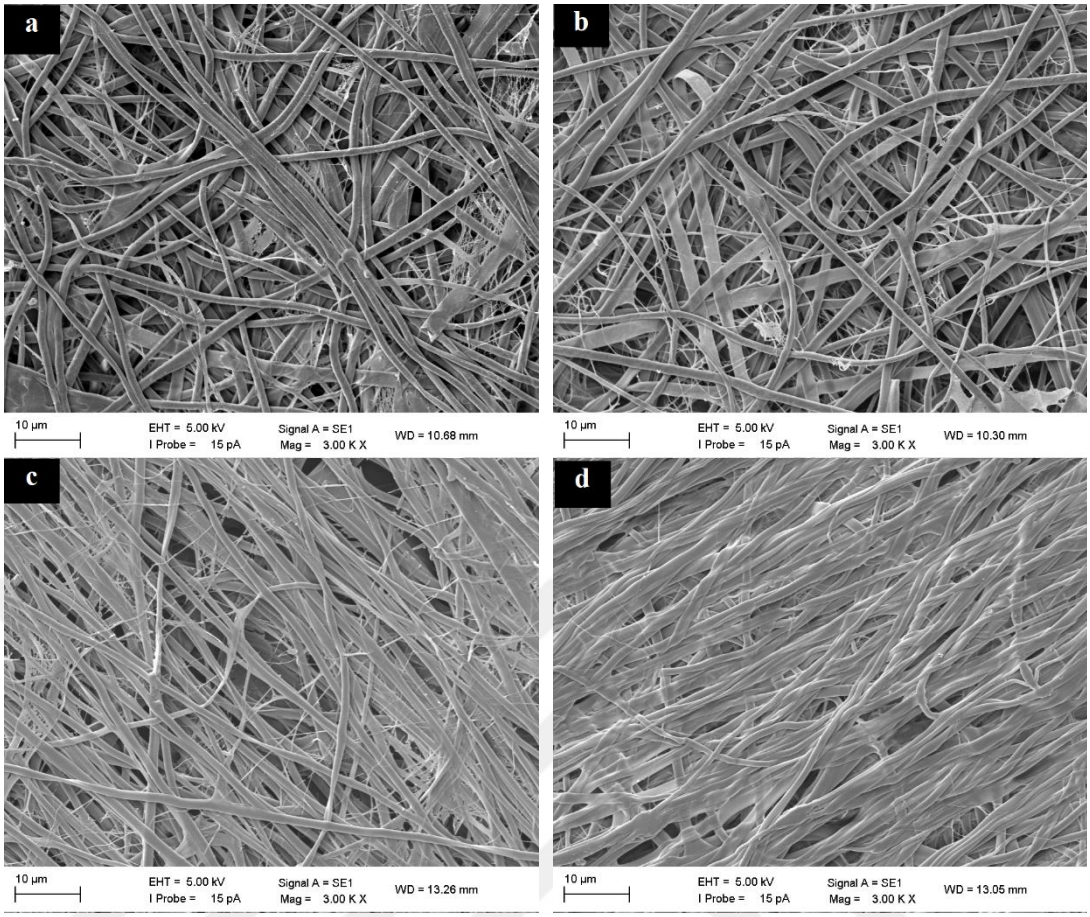

Figure 18 SEM images of electrospun fibrous mats obtained by electrospinning. (a) Run X; (b) Run XI; (c) Run XII and (d) Run XIII. Magnification x3000; scale bar 10 µm.

To prevent the fusion of the fibers due to mandrel's speed being too high, an electrospinning run at 2500 rpm (Run XIV) was done. The mat had fibers that were mainly aligned with the occasional random fiber.

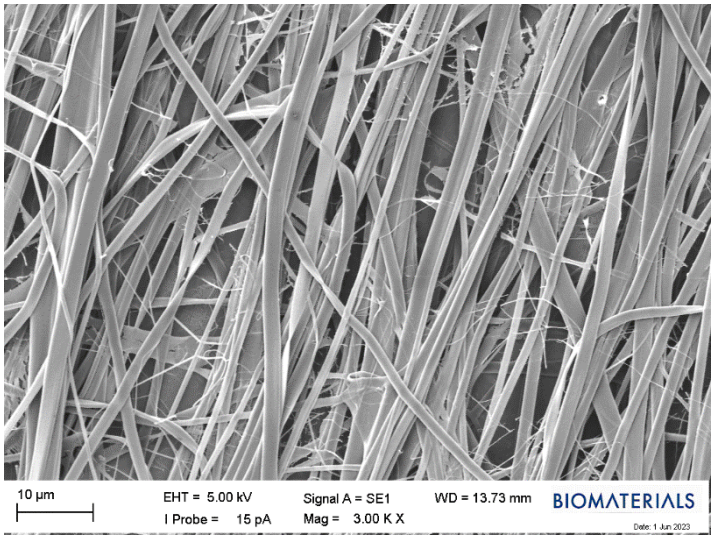

Figure 19 SEM image of electrospun fibrous mat obtained by electrospinning, Run XIV. Magnification x3000; scale bar 10 µm

4.2.2 Fiber Diameter and Orientation Analysis

The orientation of the fibers and their diameters were analyzed using the FibroQuant 1.3 software. The diameters of the mat fibers ranged from 40 to 990 nm (Figure 20a), with the fibers of the largest fraction (24.3%) having a diameter at the range of 110-170 nm. It can be stated that the fiber diameter was mainly in the range of 110-360 nm, even though fibers as thick as 1 µm were obtained. The orientation of the fibers was calculated from the SEM images at 0º-15º and 15º-45º deviation angles. Since deviation at 0-15º is accepted as "aligned", about 30% of the fibers was considered aligned (Figure 20b).

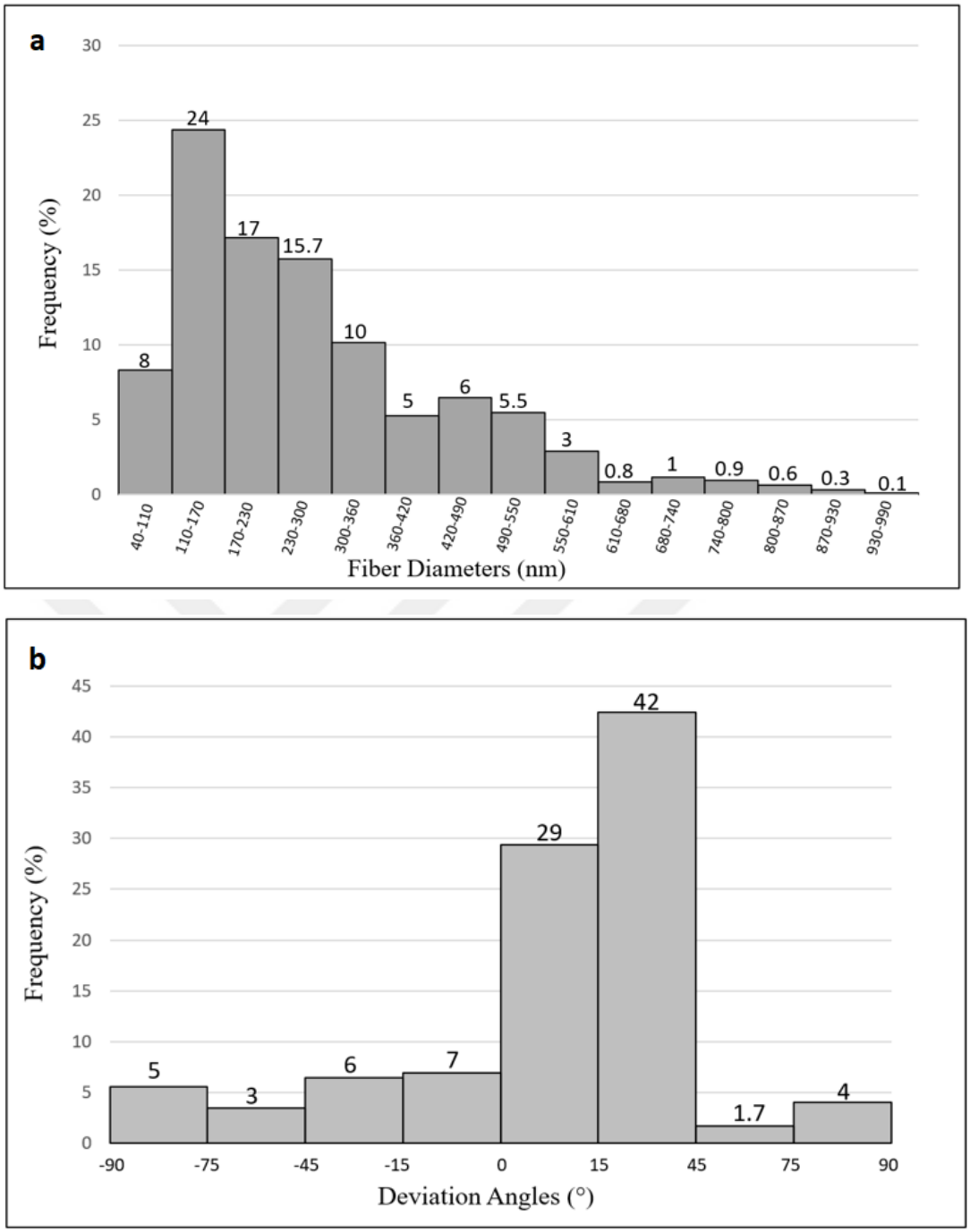

Figure 20 The fiber analysis. (a) Fiber diameter, and (b) Fiber deviation angles

4.2.3 Mechanical Analysis

Tensile testing was done on samples (1 cm x 4 cm) to determine the mechanical properties of the electrospun fiber mats. A stress-strain curve was obtained from which the tensile modulus of the samples was calculated to be 1499 ± 200 MPa, while the ultimate tensile stress and ultimate tensile strain were calculated, respectively as 51.6 MPa and 7.5% (Figure 21). The natural ACL tissue has a Young's modulus of 204.1 ± 89.5 MPa and an ultimate tensile stress of 39.6 ± 5.5 MPa [101], the values of the fiber mat produced were much higher than the native tissue showing that the electrospun SF-Col1 mat can perform as a scaffold for ACL tissue engineering.

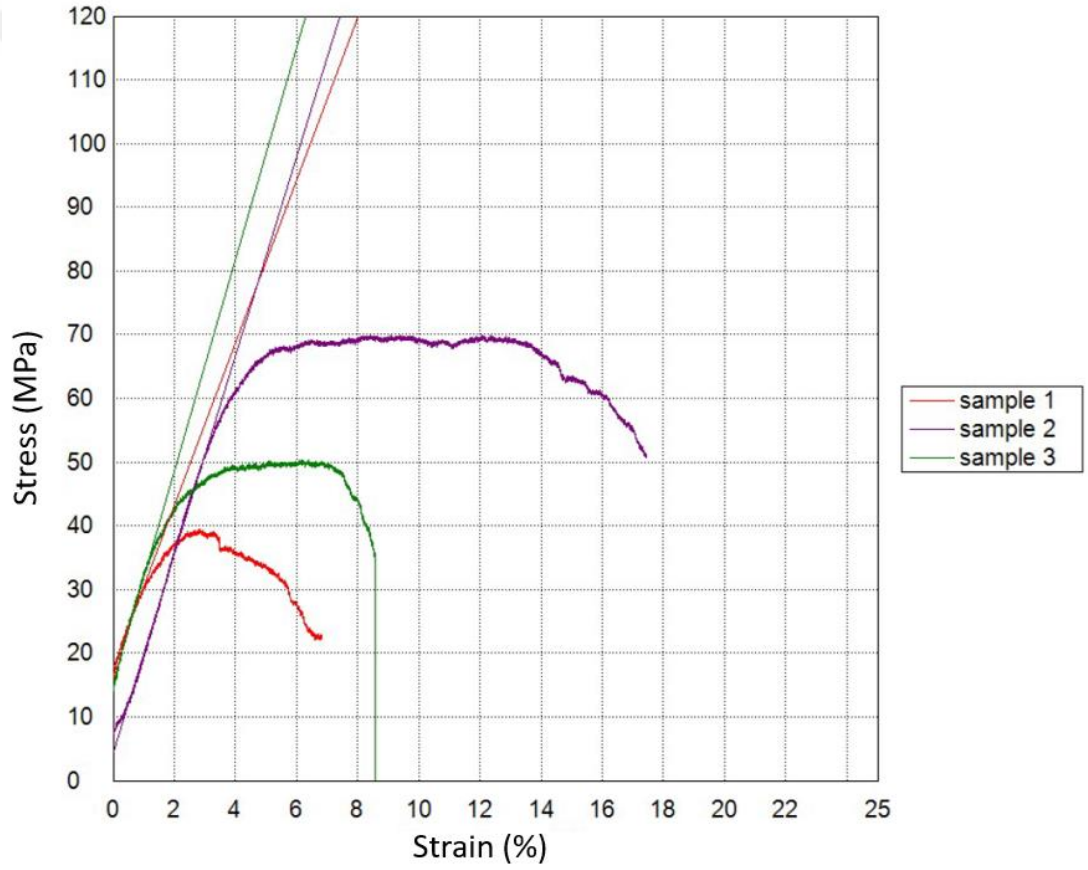

Figure 21 Stress-Strain Curves of the Electrospun Fiber Mats (n=3).

4.3 Characterization of the GelMA Hydrogel

4.3.1 ^{1}H-Nuclear Magnetic Resonance (^{1}H-NMR) Spectrum of GelMA

In order to calculate the degree of methacrylation, the ^{1}H-NMR spectrum of both the gelatin used for the synthesis of GelMA and the methacrylated GelMA polymer were obtained. The resulting spectra (Figure 22) were examined with MestreNova NMR analysis software (version 6.0.2, Mestrelabs Research) to calculate the methacrylation degree. Methacrylate gives two peaks between 5.5-6 ppm while phenylalanine gives a peak between 7.5-6.9 ppm, after methacrylation this peak remains unchanged. Due to this, both spectra were normalized according to the phenylalanine's peak. Lysine peaks in between 2.95-2.8 ppm were used to calculate the methacrylation degree according to the equation given in Section 3.2.2.1. The methacrylation degree of the GelMA used in this study was found as 98.4%.

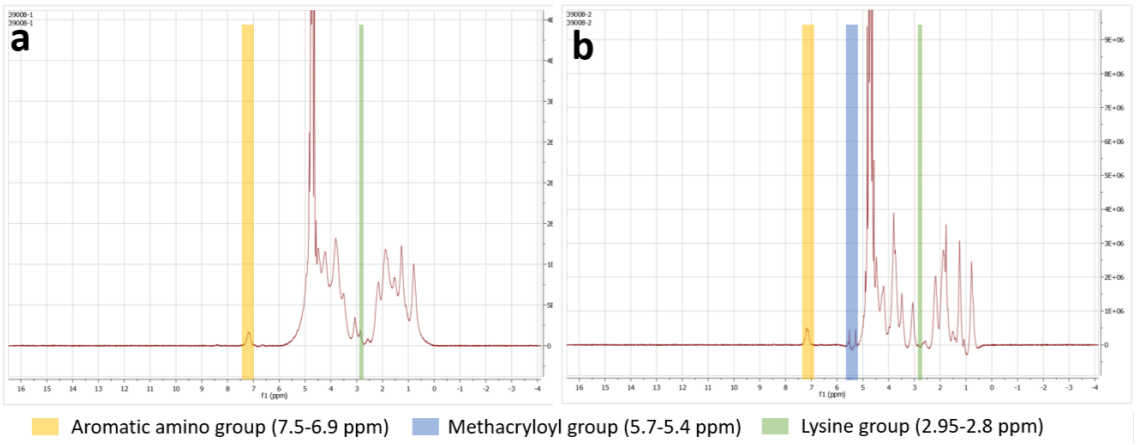

Figure 22 ^{1}H-NMR Spectra. a) Gelatin, and b) GelMA.

4.3.2 Equilibrium Water Content (EWC) of GelMA

Hydrogels are polymeric structures that are highly hydrophilic, and this property allows these materials to withhold large amounts of water. The water retention property of an hydrogel is important as it directly affects its mechanical strength when swollen and its porosity [102]. For the GelMA slab samples (n=5) prepared with 16% GelMA concentration with 2 min UV exposure, the equilibrium water content was calculated as 84.8 %, showing high hydrophilicity while the water content of the

natural tissue ranges in between 60-80% [13]. The hydrogels produced have a slightly higher water retention level compared to the ACL tissue.

4.3.3 Mechanical Analysis of GelMA Slabs

The GelMA slabs were tested through compression to determine the mechanical properties of the hydrogel. The samples (5 mm height, 3 mm diameter) were tested with 0.5 mm/min test speed. A stress-strain curve was drawn for each sample and the compressive modulus was calculated (Figure 23). The compressive modulus of the samples were calculated as 308 ± 23 kPa, quite similar to the modulus values found in the literature of the similar GelMA studies [103].

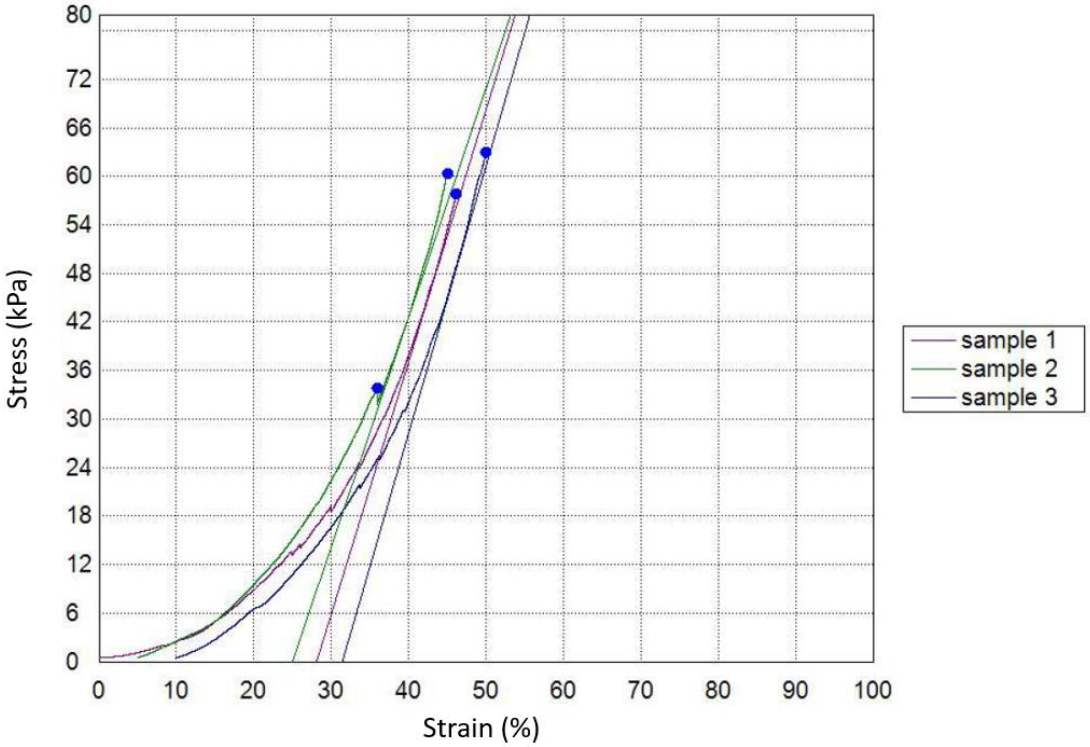

Figure 23 Stress-Strain curves of GelMA slabs (n=3).

4.4 Characterization of the Bilayered GelMA-Electrospun Fiber Tube

The bilayered tubes were produced by rolling a bilayered construct composed of a GelMA layer and electrospun fiber layer into a tubular shape (Figure 24). The diameter of the tubes was 4.86 ± 0.43 cm and its length was 1.78 ± 0.14 cm.

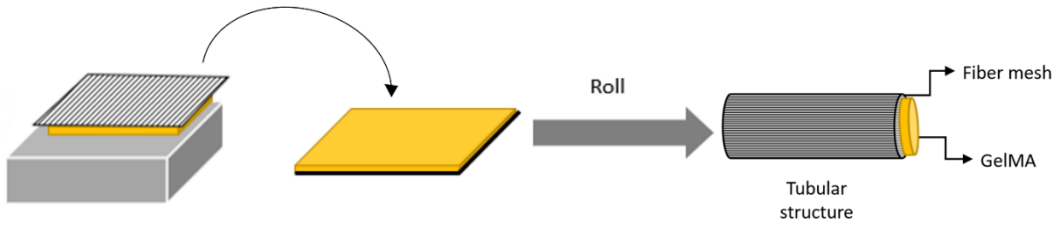

Figure 24 Preparation of Bilayered GelMA-Electrospun Fiber Tube.

4.4.1 Scanning Electron Microscopy (SEM)

The tubular structure was examined with Scanning Electron Microscopy (Thermo Quatro ESEM) under low vacuum conditions to observe the tubular structure with its hydrogel at a hydrated state. One of the samples was cut diagonally to examine the two layers (Figure 25), while in another tubular sample was examined as a whole (Figure 26).

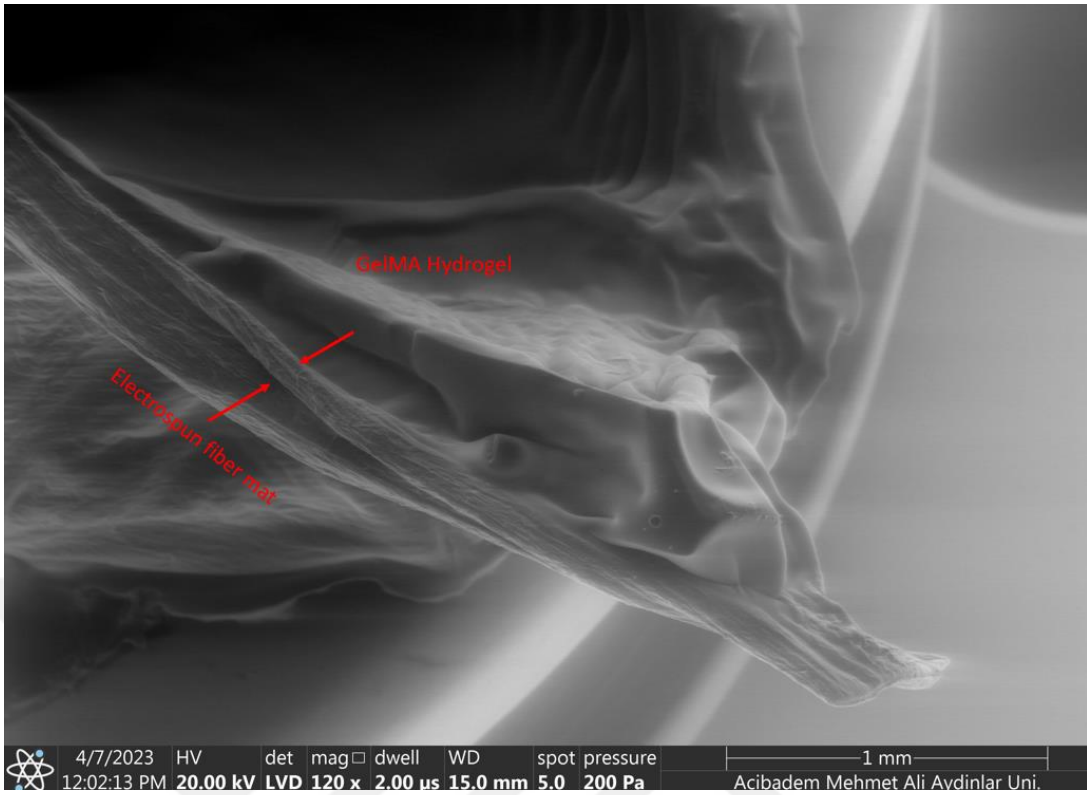

Figure 25 SEM image of the two layers of the tubular structure under low vacuum. Magnification: x120, Scale bar: 1 mm.

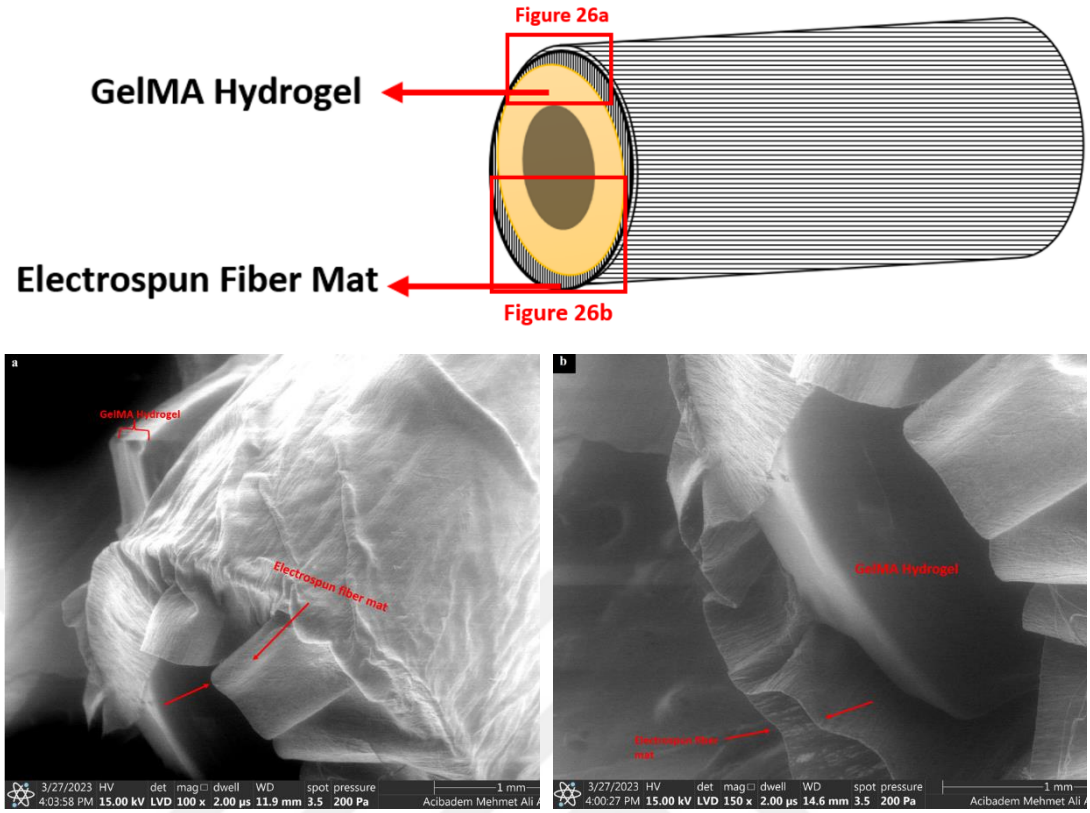

Figure 26 SEM images of the tubular structure. a) The top view, b) Frontal view, Magnification: x120, Scale bar: 1 mm.

After the sample was freeze dried, a section of it was cut to have it examined under SEM. In the images, the two layers made up of GelMA hydrogel and electrospun fiber mat can be seen (Figure 27b). In the GelMA hydrogel layer, the interconnected porous structure could be observed.

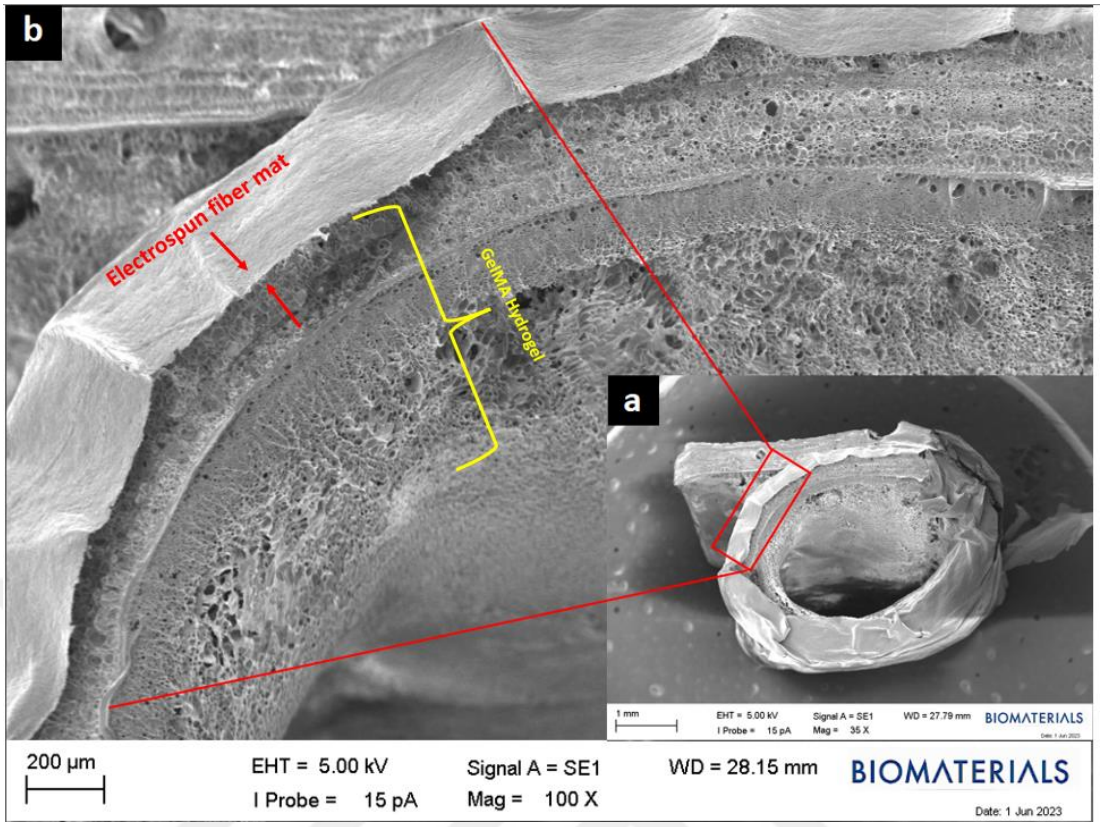

Figure 27 SEM images of the tubular structure. (a) The upper view, Magnification: x35, Scale bar: 1 mm; (b) Close-up of the wall of the tube, Magnification: x100, Scale Bar: 200 µm

4.5 *In vitro* Studies

4.5.1 Live-Dead Cell Viability of GelMA Slabs

Live-Dead Assay was done to the cell loaded GelMA hydrogels to observe the viability of the cells within the intended hydrogel concentration and whether the time exposed to UV to crosslink GelMA had any negative effects on cell survival. After 8 days in culture, the assay was performed on the samples. The images of the living cells (green) and dead cells (red) were obtained with CLSM (Zeiss LSM 900, Germany). Z-stacks at x10 magnification (Figure 29) were taken from both sides of the slabs. For the bottom of the slabs, a higher amount of dead cells were observed (Figures 28(a-b) and 29(b)).

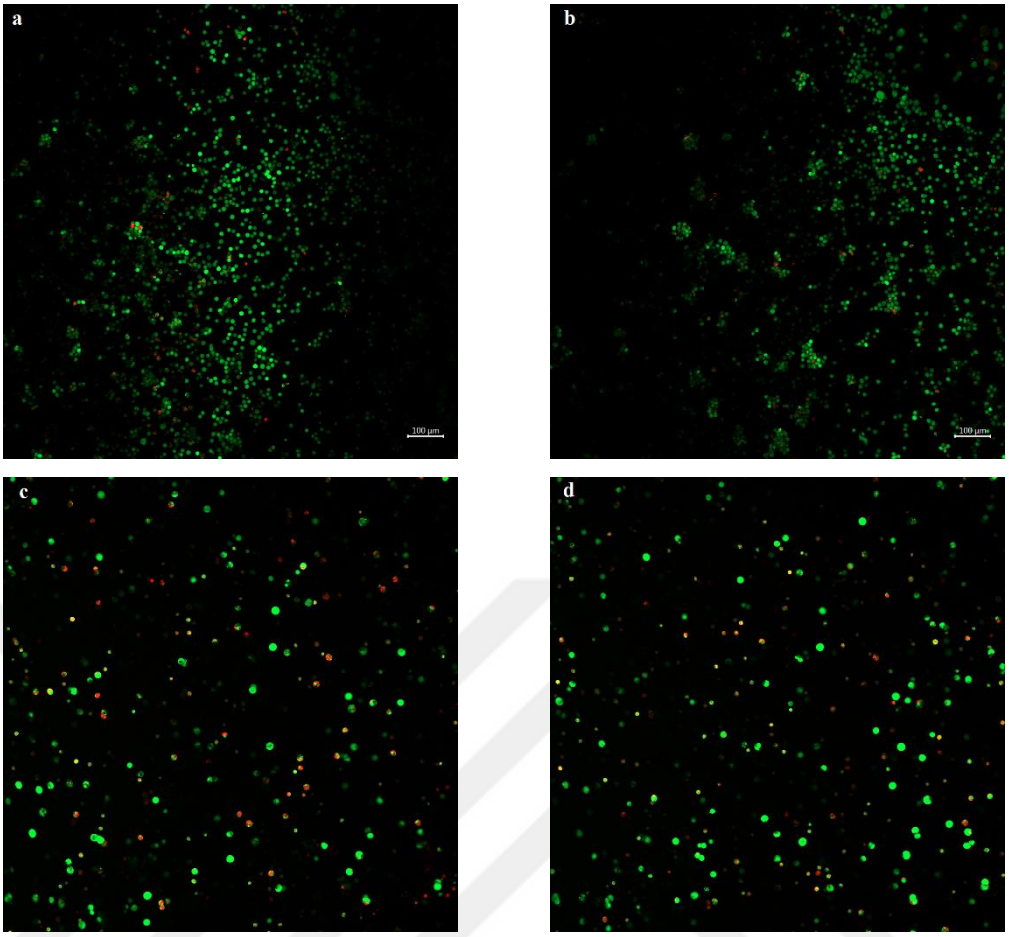

Figure 28 CSLM images of the Live-Dead Cell Viability Assay of GelMA hydrogel slabs on Day 8. (a-b the top of the slab, (c-d) bottom of the slab. Magnification: x10; scale bar 100 μm

For the calculation of the cell viability, the z-stack image of the total slices taken from both sides were used (Figure 28) and the viability of the cells was calculated according to the equation given in Section 3.2.4.3. The fraction of the living cells was calculated to be 83%. The cell viability (with the parameters the concentration of GelMA and time under UV exposure) for the GelMA hydrogel slab was decided to be acceptable since for cellular viability fraction ≥70% are considered acceptable for cellular viability. Due to this, for the rest of the *in vitro* studies the same hydrogel preparation parameters were applied.

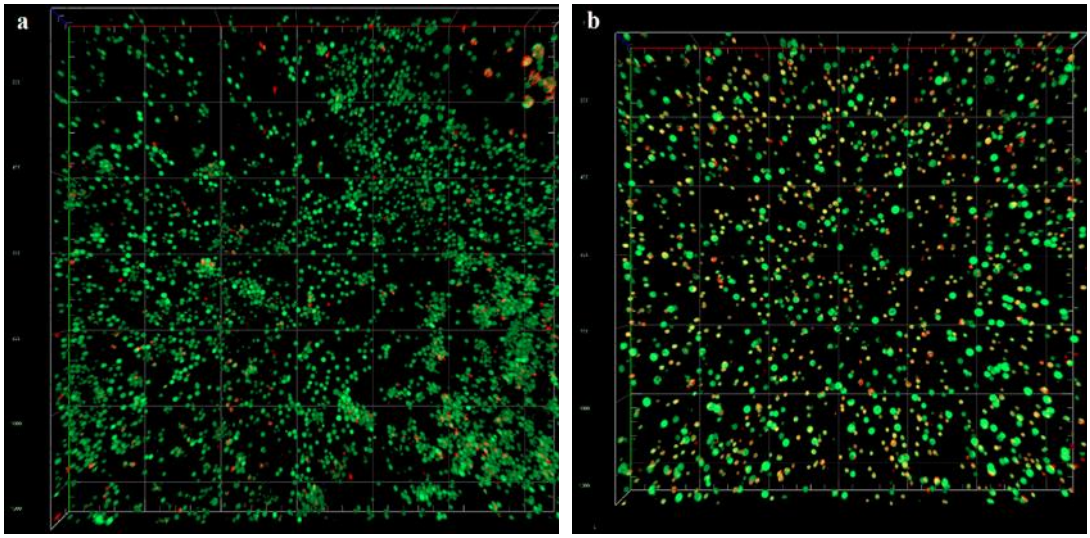

Figure 29 z-Stack CSLM images of the Live-Dead Cell Viability Assay of GelMA hydrogel slabs on Day 8. (a) top; (b) bottom; Magnification: x10, Scale bar: 300 μm.

4.5.2 Alamar Blue Assay of the Cells in the Tubular Structure

Alamar Blue Assay's of the samples (n=3) were measured on Days 1, 3, 7 and 14. Using the equation given in Section 3.2.4.5.1, the percentage of the reduced resazurin was calculated and a graph (Figure 29) was drawn. In the first 7 days of culture, the cells showed a linear growth in their proliferation rate. The continuous reduction of the resazurin, shows that the cells were able to proliferate while in the tubular structure and thus continue with their cellular activities.

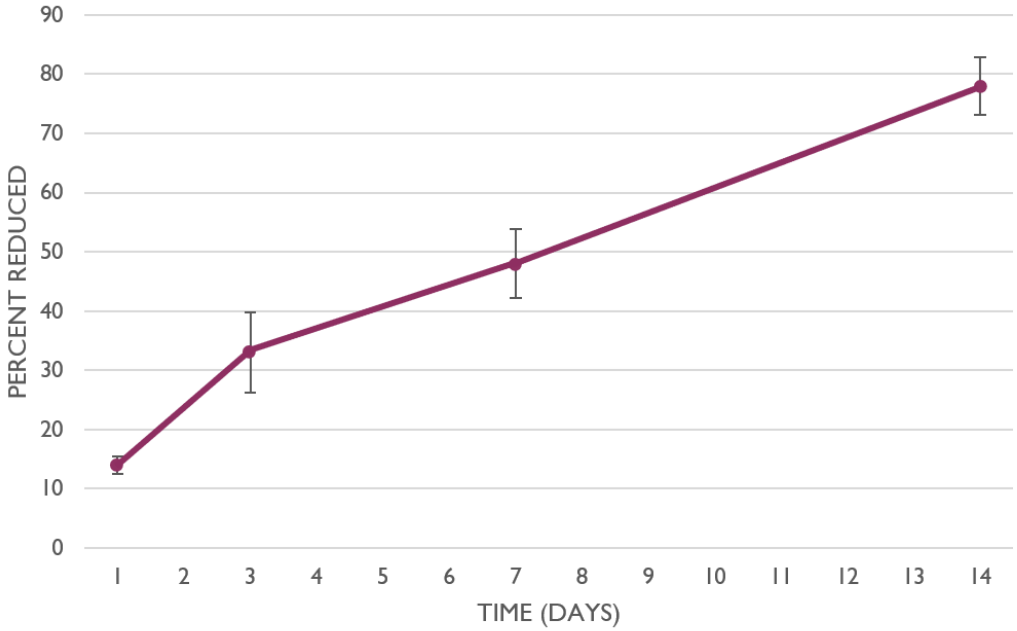

Figure 30 Alamar Blue Assay results of the samples (n=3).

4.5.3 Live-Dead Cell Viability of the Tubular Structure

Live-Dead Cell Viability Assay was carried out on the tubular samples on the Days 3 and 14 of the culture and especially the GelMA layer of the samples were examined as the cells were most abundant there (Figure 31).

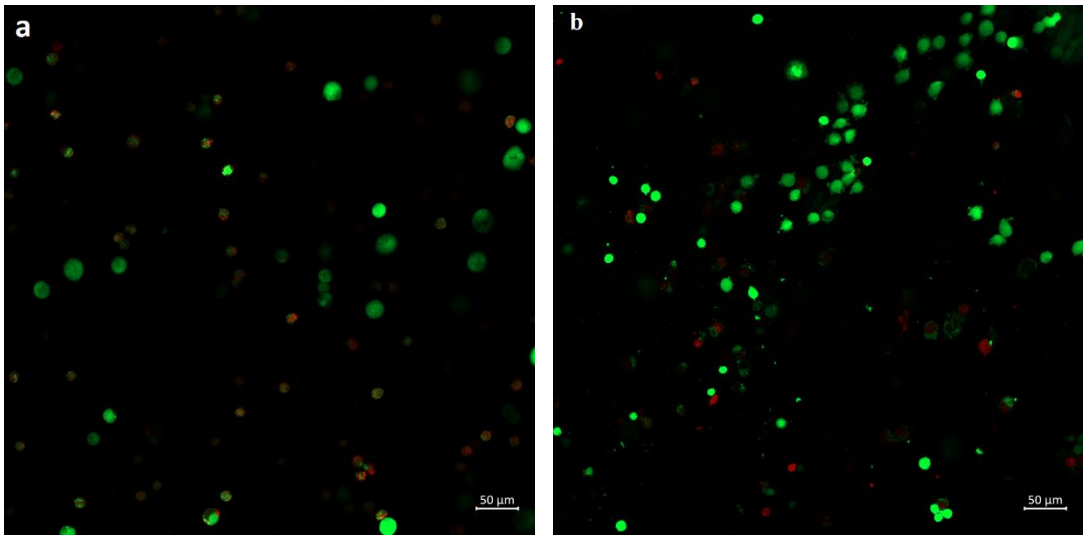

Figure 31 CLSM images of the Live-Dead Cell Viability Assay of the GelMA hydrogel layer of the tubular structure. (a) Day 3 and (b) Day 14. Magnification: x10, Scale bar: 50 µm.

For the calculation of the cell viability, the z-stack images of the total slices were used (Figure 32). On Day 3, cell viability was 68.8% while for Day 14 this value increased to 88.8%. The lower viability of the cells on Day 3 can be attributed to the mechanical stress the cells were exposed to on Day 1 where the bilayered slab was rolled into a tubular structure.

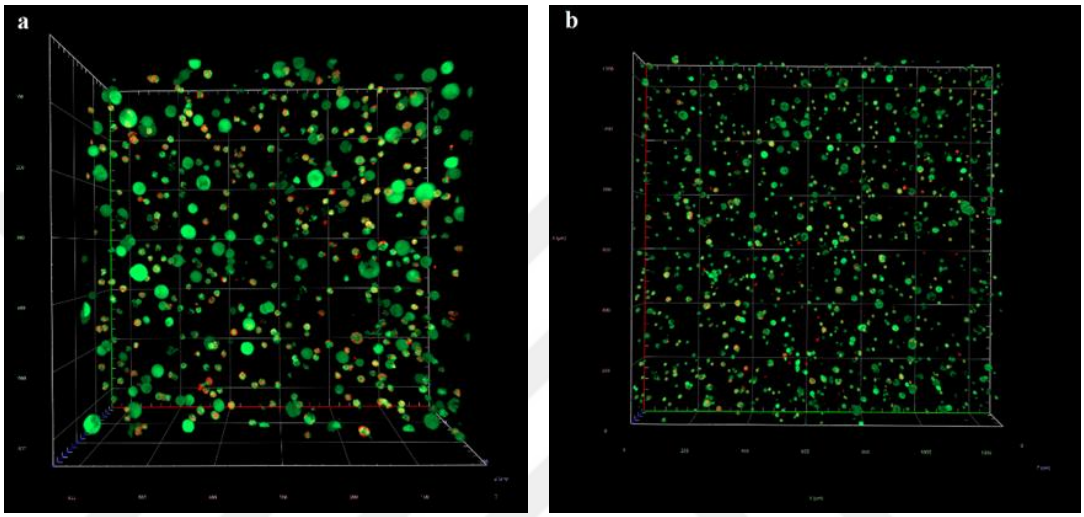

Figure 32 z-Stack CLSM images of the Live-Dead Cell Viability Assay of GelMA hydrogel layer. (a) Day 3; (b) Day 14; Magnifications: x10, Scale bar: 300 μm.

4.5.4 Phalloidin-DAPI Staining of the Tubular Structure

The tubular samples were stained with FITC conjugated Phalloidin and DAPI to examine the morphology of the cells within the bilayered tubes. The samples were fixed on Days 3 and 14 with 4% PFA, and after staining the samples were examined under CLSM (Zeiss LSM 900, Germany). The cellular morphology within the structure as a whole, and separately both on the fiber and hydrogel layers were examined. On the images taken together with the electrospun fiber mat the nuclei of the cells could not be seen. This may be due to the auto-immunofluorescence of the silk fibroin used for the fabrication of the electrospun fiber mats. DAPI, the dye that stains the nuclei of the cells has a blue color at 358 nm, when during examination with CSLM under the wavelength required to observe the staining the signal caused by the

auto-fluorescent properties of silk fibroin [104] may be suppressing the signal of the stained nuclei and preventing them from being observed (Figures 34(b) and 36(c-d)). When comparing Day 3 (Figures 33-34) to Day 14 (Figures 35-36), the L929 cells showed a continued proliferation as it could be seen from the increased number of cells in the GelMA layer (Fig. 36a).

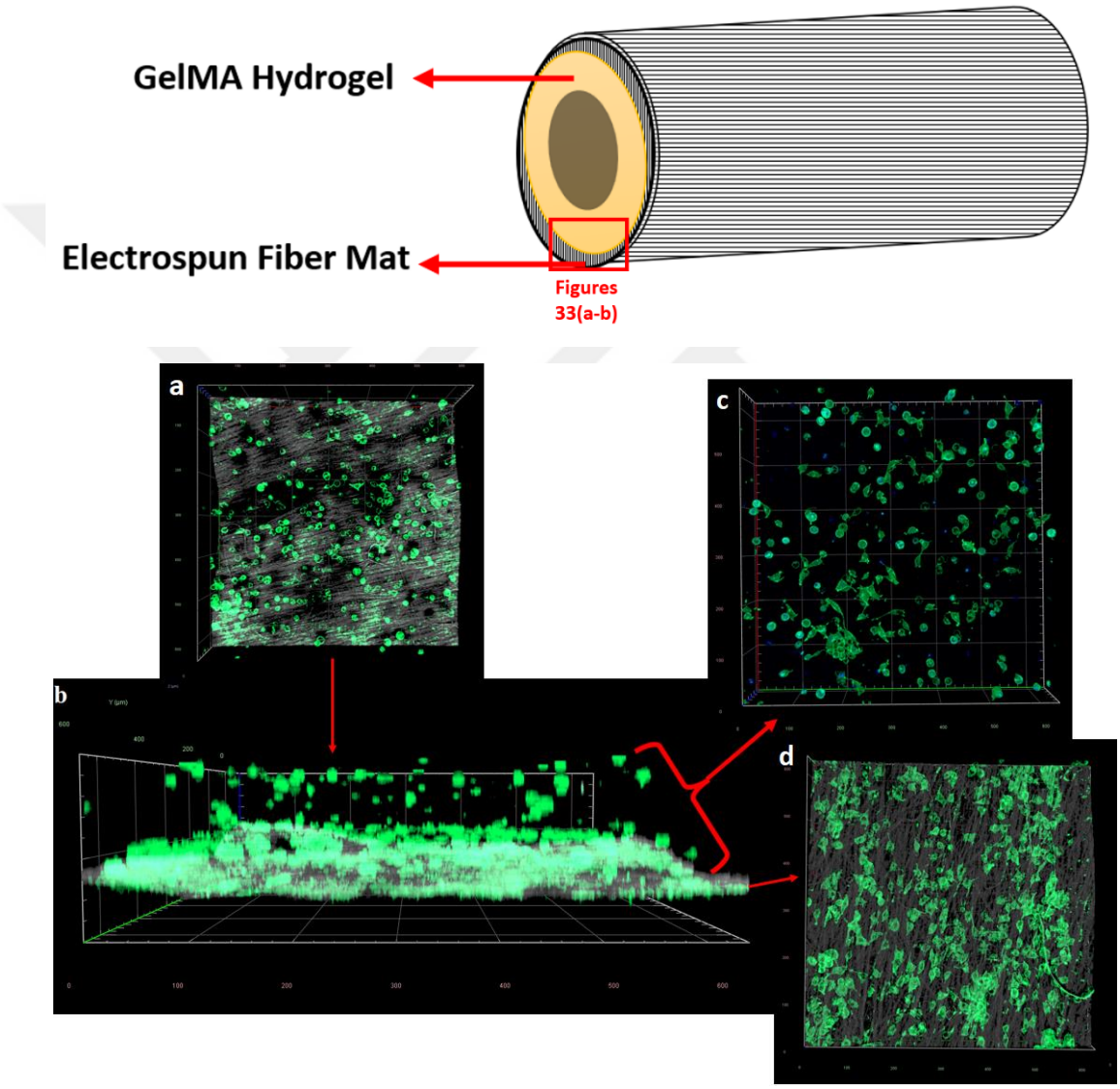

Figure 33 z-Stack CLSM images of the Phalloidin-DAPI staining of the tubular structure at Day 3. (a) Top view of the tubular structure; (b) Side view of the tubular structure; (c) GelMA layer; (d) Electrospun fiber layer; Magnifications: x10, Scale bar: 300 μm

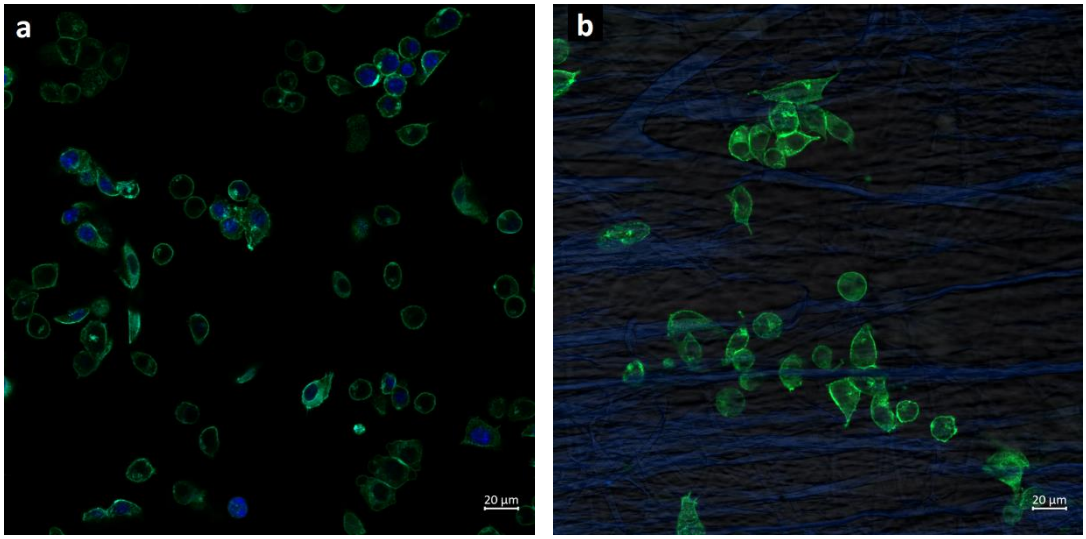

Figure 34 CLSM images of the Phalloidin-DAPI staining on Day 3. (a) GelMA layer, (b) Electrospun fiber layer. Magnification: x20, Scale bar: 20 µm

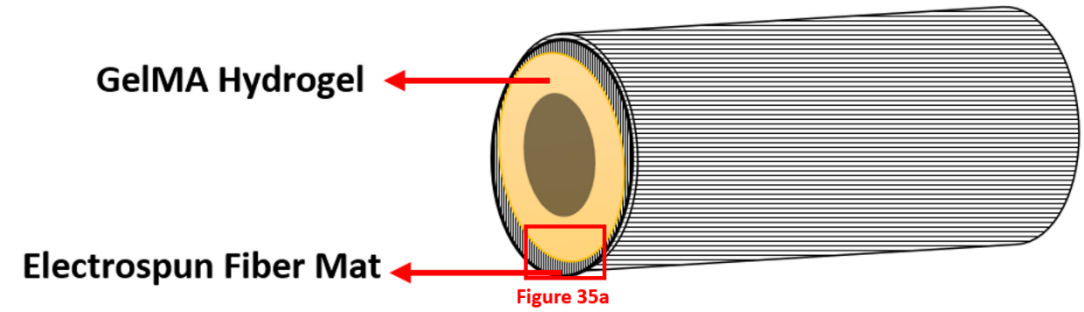

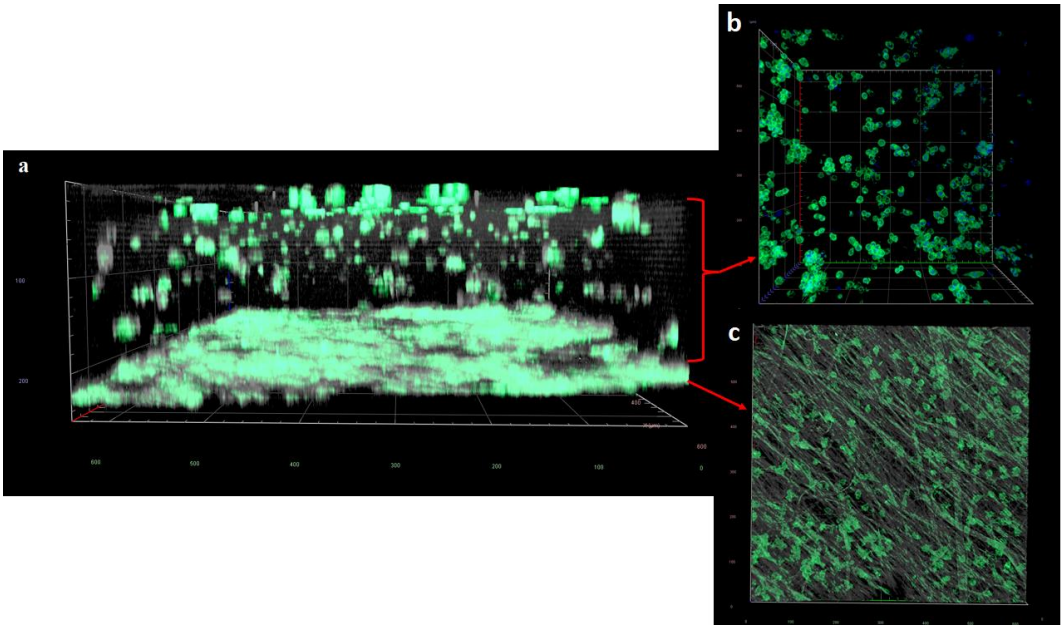

Figure 35 z-Stack CLSM images of the Phalloidin-DAPI staining of the tubular structure on Day 14. (a) The side view of the tubular structure, (b) GelMA layer, (c) Electrospun fiber layer. Magnification: x10, Scale bar: 300 μm.

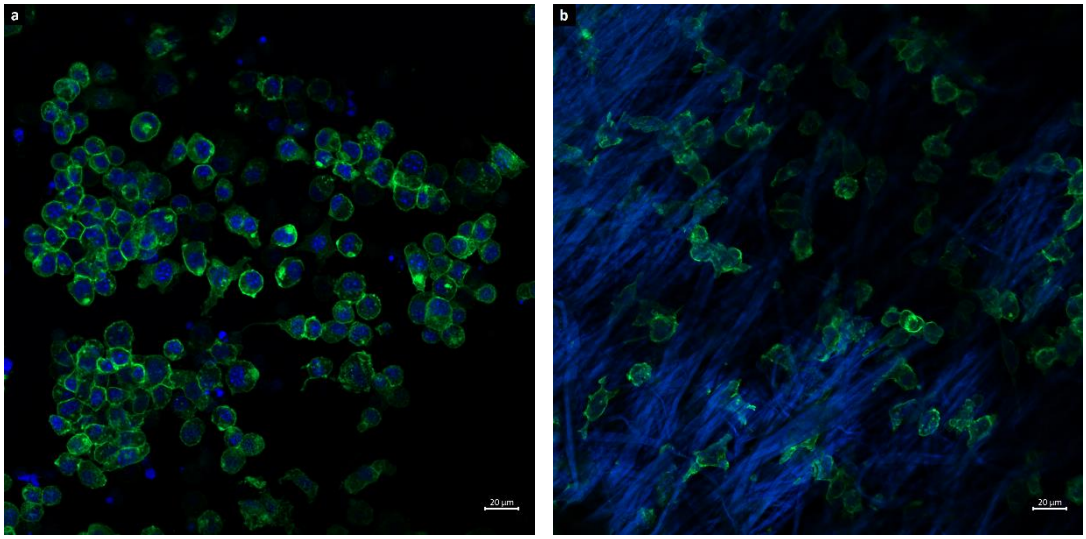

Figure 36 CLSM images of the Phalloidin-DAPI staining on Day 14. (a) GelMA layer, and (b) Electrospun fiber layer; Magnification: x20, Scale bar: 20 µm.

5 DISCUSSION

In this study, silk fibroin and collagen type I were chosen as the polymer for electrospinning to produce a mat with aligned fibers. Collagen Type I was chosen due to its abundance in the natural tissue and silk fibroin was chosen to give mechanical support. A layer composed of GelMA hydrogel loaded with cells were then combined with the electrospun fiber mat. This bilayered structure was then rolled up to a tubular shape to imitate the shape of the ligament. Two 3D printed rings made from PLA were used to keep the bundle in tubular shape. L929 fibroblast cells were used throughout this study as they are the most abundant cells found in native ACL tissue [13].

A fiber mat with aligned fiber orientation was produced through electrospinning. The structure of ACL is made up of fascicles (250 μm diameter) of multiple bundled collagen fibrils of 25-250 nm diameters that are parallel to each other [13-15]. The diameters of electrospun mat's fibers were between 40 nm-1 μm, with the fibers with thickness in the range of 110-360 nm making up most of the mat. The fibers were highly oriented (0-15^{o} and 15-45^{o}), as a deviation of 15^{o} is considered as aligned and here about 30% of the fibers were aligned. When compared with the natural tissue, the produced electrospun mat had fiber thickness similar to the ACL, while in some other studies where an electrospun fiber mat of SF-ColI had much thicker fibers with 910 ± 60 nm diameter [96]. In another study, a SF-PEO electrospun mat had a fiber thickness of 700 ± 50 nm [94].

ACL is crucial part of the knee, functioning as the stabilizer of the joint [7], bearing high mechanical loads. After a tear, the tissue can not heal itself or continue its function at its previous performance level [53-55]. Due to this, through reconstruction surgery, the stumps of the ligaments are shaved off and a graft made from tendons is passed through the holes drilled into the femur and tibia [5, 59]. These grafts depending on where the tendon is harvested from have different mechanical properties. The bone-patellar tendon-bone, the most preferred graft of the surgeons, has a Young's modulus of 297 MPa, while for hamstring tendons this value is 557 MPa [105] and for the natural ACL it is 204.1 MPa [101]. The electrospun fiber produced in this study, had a much higher Young's modulus (1.499 GPa) when

compared to both the native ACL and the graft alternatives. A mat prepared by electrospinning of SF-Col1 had a much weaker modulus of 9.78 MPa [96]. Comparing the ultimate tensile stress value of the fiber mat to that of the natural ACL tissue, the fiber mat had a higher value (51.6 MPa) compared to ACL (39.6 MPa) and is therefore very suitable for the purpose [101].

In order to mimic the ECM of the native tissue and to act as the cell carrying layer, GelMA polymer was synthesized by the methacrylation of gelatin. The methacrylation degree was calculated by ^{1}H-NMR spectra of the gelatin used in the synthesis reaction and the methacrylated GelMA polymer. For the GelMA used throughout this study, the methacrylation degree was calculated as 98.4%. A high methacrylation degree (≥ 80%) for GelMA produces a hydrogel with increased stiffness whilst decreasing the equilibrium water content [106]. For the 16% GelMA, the EWC was calculated as 84.8% and with a compressive modulus of 308± 23 kPa, showing that the hydrogel had sufficient hydrophilicity allowing solutions to enter whilst still retaining its mechanical properties.

As the cell carrier layer, the GelMA hydrogel layer needed to have enough cell attracting properties to retain the cells while not affecting the proliferation and viability of the cells. To determine the viability of cells within GelMA hydrogel slabs, Live-Dead Assay was conducted on L929 loaded hydrogel slabs. After 8 days in culture, the viability was calculated as 83%, with the bottom of the slab having a higher proportion of dead cells which may be due to being exposed to poor culture conditions (low O_2 and nutrient) throughout the incubation. With an acceptable level of the cells staying alive after culture, the parameters for the GelMA hydrogel with 16% (w/v) GelMA concentration and 2 min UV was used for *in vitro* studies with bilayered tube.

A bilayered tube made up of a cell-loaded GelMA layer and a SF-ColI electrospun fiber mat was prepared. During *in vitro* studies, in order to prevent the tube from uncoiling, rings were placed at both ends. By conducting Alamar Blue Assay, Live Dead Assay and Phalloidin-DAPI Staining the proliferation, viability and morphology of the cells were determined respectively. On Day 3, there was a high amount of dead

cells (32%) but as the culture progressed to Day 14 the viability of the cells increased to 88%. This difference may be caused by the mechanical stress applied to the cells during the rolling and placing the rings. The increased viability on Day 14 show that while initially rolling the tube negatively affected the cell viability in time the cells were able to overcome this effect. For the cell proliferation, the cells had a linear growth through the Days 1-7, and after Day 7 of culture there was a distinct increase, possibly caused by the cells overcoming the stress at the start of culture. Cellular morphology did not change significantly between Day 3 and Day 14. Unlike most fibroblasts which are spindle shaped [107] L929 exhibits a round morphology, but the increase in cell numbers could be seen along with the attachment of cells to the fiber layer.

6 CONCLUSION

In this thesis, the aim was to develop a tissue engineered ACL through electrospinning. The electrospun fiber mat with aligned fibers were produced with silk fibroin and collagen type I as the polymer, this fiber mat was then combined with GelMA loaded with L929 fibroblast cells. This bilayered construct was then rolled to give it a tubular shape to achieve a suturable implant.

The viability of cells within GelMA and the tubular structure was determined through various *in vitro* assays. The Live-Dead Cell Viability assay results showed that GelMA concentration, along with the duration of exposure to UV, did not affect the cell viability and proliferation after 8 days in culture, and with the tubular construct both Live-Dead Cell Viability and Alamar Blue assays showed that cells continued their cellular activity and proliferation for the 14 day culture duration.

The fiber layer of the construct showed viscoelastic mechanical properties with a high Young's modulus surpassing that of the native tissue.

In the future, other materials could be introduced to the fiber structure to improve elasticity. Improvements could be made to preserve the tubular shape of the construct in *in vitro* studies during this study 3D printed PLA rings were used to keep the bundle in tubular shape.

In conclusion, the tubular structure appears to be capable of maintaining cellular viability and proliferation, and therefore, *in vivo* studies could be initiated.

7 REFERENCES

1. Cimino F, Volk BS, Setter D. Anterior cruciate ligament injury: diagnosis, management, and prevention 2010.

2. Kaeding CC, Leger-St-Jean B, Magnussen RA. Epidemiology and Diagnosis of Anterior Cruciate Ligament Injuries 2017.

3. Filbay SR, Grindem H. Evidence-based recommendations for the management of anterior cruciate ligament (ACL) rupture. Best Pract Res Clin Rheumatol. 2019;33(1):33-47.

4. West RV, Harner CD. Graft selection in anterior cruciate ligament reconstruction. J Am Acad Orthop Surg. 2005;13(3):197-207.

5. Siegel L, Vandenakker-Albanese C, Siegel D. Anterior cruciate ligament injuries: anatomy, physiology, biomechanics, and management. Clin J Sport Med. 2012;22(4):349-55.

6. Langer R, Vacanti J. Advances in tissue engineering. J Pediatr Surg. 2016;51(1):8-12

7. Abulhasan J, Grey M. Anatomy and physiology of knee stability. Journal of Functional Morphology and Kinesiology. 2017;2(4):34.

8. Hirschmann MT, Muller W. Complex function of the knee joint: the current understanding of the knee. Knee Surg Sports Traumatol Arthrosc. 2015;23(10):2780-8.

9. Hassebrock JD, Gulbrandsen MT, Asprey WL, Makovicka JL, Chhabra A. Knee Ligament Anatomy and Biomechanics. Sports Med Arthrosc Rev. 2020;28(3):80-6.

10. Zantop T, Petersen W, Sekiya JK, Musahl V, Fu FH. Anterior cruciate ligament anatomy and function relating to anatomical reconstruction. Knee Surg Sports Traumatol Arthrosc. 2006;14(10):982-92.

11. Petersen W, Zantop T. Anatomy of the anterior cruciate ligament with regard to its two bundles. Clin Orthop Relat Res. 2007;454:35-47.

12. Zantop T, Petersen W, Fu FH. Anatomy of the anterior cruciate ligament. Operative Techniques in Orthopaedics. 2005;15(1):20–8..

13. Duthon VB, Barea C, Abrassart S, Fasel JH, Fritschy D, Menetrey J. Anatomy of the anterior cruciate ligament. Knee Surg Sports Traumatol Arthrosc. 2006;14(3):204-13.

14. Marieswaran M, Jain I, Garg B, Sharma V, Kalyanasundaram D. A Review on Biomechanics of Anterior Cruciate Ligament and Materials for Reconstruction. Appl Bionics Biomech. 2018;2018:4657824.

15. Dienst M, Burks RT, Greis PE. Anatomy and biomechanics of the anterior cruciate ligament. Orthop Clin North Am. 2002;33(4):605-20, v.

16. Banu J, Sontakke Y, Tamgire D, H Y S. Histological structure of anterior cruciate ligament - review. Academia Anatomica International. 2019;5(1).

17. Petersen W, Tillmann B. Structure and vascularization of the cruciate ligaments of the human knee joint. Anat Embryol (Berl). 1999;200(3):325-34.

18. Scapinelli R. Vascular anatomy of the human cruciate ligaments and surrounding structures. Clin Anat. 1997;10(3):151-62.

19. Kennedy JC, Alexander IJ, Hayes KC. Nerve supply of the human knee and its functional importance. Am J Sports Med. 1982;10(6):329-35.
20. Schultz RA, Miller DC, Kerr CS, Micheli L. Mechanoreceptors in human cruciate ligaments. A histological study. J Bone Joint Surg Am. 1984;66(7):1072-6.
21. Hogervorst T, Brand RA. Mechanoreceptors in joint function. J Bone Joint Surg Am. 1998;80(9):1365-78.
22. Gianotti SM, Marshall SW, Hume PA, Bunt L. Incidence of anterior cruciate ligament injury and other knee ligament injuries: a national population-based study. J Sci Med Sport. 2009;12(6):622-7.
23. Kiapour AM, Murray MM. Basic science of anterior cruciate ligament injury and repair. Bone Joint Res. 2014;3(2):20-31.
24. The female ACL: Why is it more prone to injury? J Orthop. 2016;13(2):A1-4.
25. Yu WD, Panossian V, Hatch JD, Liu SH, Finerman GA. Combined effects of estrogen and progesterone on the anterior cruciate ligament. Clin Orthop Relat Res. 2001(383):268-81.
26. Mandelbaum BR, Silvers HJ, Watanabe DS, Knarr JF, Thomas SD, Griffin LY, et al. Effectiveness of a neuromuscular and proprioceptive training program in preventing anterior cruciate ligament injuries in female athletes: 2-year follow-up. Am J Sports Med. 2005;33(7):1003-10.
27. Zazulak BT, Paterno M, Myer GD, Romani WA, Hewett TE. The effects of the menstrual cycle on anterior knee laxity: a systematic review. Sports Med. 2006;36(10):847-62.
28. Wang HM, Shultz SJ, Schmitz RJ. Association of Anterior Cruciate Ligament Width With Anterior Knee Laxity. J Athl Train. 2016;51(6):460-5.
29. Beynnon BD, Johnson RJ, Braun S, Sargent M, Bernstein IM, Skelly JM, et al. The relationship between menstrual cycle phase and anterior cruciate ligament injury: a case-control study of recreational alpine skiers. Am J Sports Med. 2006;34(5):757-64.
30. Griffin LY, Albohm MJ, Arendt EA, Bahr R, Beynnon BD, Demaio M, et al. Understanding and preventing noncontact anterior cruciate ligament injuries: a review of the Hunt Valley II meeting, January 2005. Am J Sports Med. 2006;34(9):1512-32.
31. Hughes G, Watkins J. A risk-factor model for anterior cruciate ligament injury. Sports Med. 2006;36(5):411-28.
32. Conley S, Rosenberg A, Crowninshield R. The female knee: anatomic variations. J Am Acad Orthop Surg. 2007;15 Suppl 1:S31-6.
33. Shambaugh JP, Klein A, Herbert JH. Structural measures as predictors of injury basketball players. Med Sci Sports Exerc. 1991;23(5):522-7.
34. Giugliano DN, Solomon JL. ACL tears in female athletes. Phys Med Rehabil Clin N Am. 2007;18(3):417-38, viii.
35. Hutchinson MR, Ireland ML. Knee injuries in female athletes. Sports Med. 1995;19(4):288-302.
36. Griffin LY, Agel J, Albohm MJ, Arendt EA, Dick RW, Garrett WE, et al. Noncontact anterior cruciate ligament injuries: risk factors and prevention strategies. J Am Acad Orthop Surg. 2000;8(3):141-50.

37. Wetters N, Weber AE, Wuerz TH, Schub DL, Mandelbaum BR. Mechanism of injury and risk factors for Anterior Cruciate Ligament Injury. Operative Techniques in Sports Medicine. 2016;24(1):2–6.
38. Walden M, Krosshaug T, Bjorneboe J, Andersen TE, Faul O, Hagglund M. Three distinct mechanisms predominate in non-contact anterior cruciate ligament injuries in male professional football players: a systematic video analysis of 39 cases. Br J Sports Med. 2015;49(22):1452-60.
39. Vahey TN, Broome DR, Kayes KJ, Shelbourne KD. Acute and chronic tears of the anterior cruciate ligament: differential features at MR imaging. Radiology. 1991;181(1):251-3
40. Stone AV, Marx S, Conley CW. Management of Partial Tears of the Anterior Cruciate Ligament: A Review of the Anatomy, Diagnosis, and Treatment. J Am Acad Orthop Surg. 2021;29(2):60-70.
41. Colombet P, Dejour D, Panisset JC, Siebold R, French Arthroscopy S. Current concept of partial anterior cruciate ligament ruptures. Orthop Traumatol Surg Res. 2010;96(8 Suppl):S109-18.
42. Hong SH, Choi JY, Lee GK, Choi JA, Chung HW, Kang HS. Grading of anterior cruciate ligament injury. Diagnostic efficacy of oblique coronal magnetic resonance imaging of the knee. J Comput Assist Tomogr. 2003;27(5):814-9.
43. Noyes FR, Mooar LA, Moorman CT, 3rd, McGinniss GH. Partial tears of the anterior cruciate ligament. Progression to complete ligament deficiency. J Bone Joint Surg Br. 1989;71(5):825-33.
44. Gordon BL. Subcommittee on Classification of Sports Injuries and Committee on the Medical Aspects of Sports. In: Standard nomenclature of athletic injuries. Chicago, Chicago: American Medical Association; 1968. p. 99–100.
45. Temponi EF, de Carvalho Junior LH, Sonnery-Cottet B, Chambat P. Partial tearing of the anterior cruciate ligament: diagnosis and treatment. Rev Bras Ortop. 2015;50(1):9-15.
46. Buckley SL, Barrack RL, Alexander AH. The natural history of conservatively treated partial anterior cruciate ligament tears. Am J Sports Med. 1989;17(2):221-5.
47. Fayard JM, Sonnery-Cottet B, Vrgoc G, O'Loughlin P, de Mont Marin GD, Freychet B, et al. Incidence and Risk Factors for a Partial Anterior Cruciate Ligament Tear Progressing to a Complete Tear After Nonoperative Treatment in Patients Younger Than 30 Years. Orthop J Sports Med. 2019;7(7):2325967119856624.
48. Peacock E. Physiology of Tendon Repair. Am J Surg. 1965;109:283-6.
49. Cottrell JA, Turner JC, Arinzeh TL, O'Connor JP. The Biology of Bone and Ligament Healing. Foot Ankle Clin. 2016;21(4):739-61.
50. Sharma P, Maffulli N. Basic biology of tendon injury and healing. Surgeon. 2005;3(5):309-16.
51. Hildebrand KA, Frank CB. Scar formation and ligament healing. Can J Surg. 1998;41(6):425-9.
52. Frank CB. Ligament structure, physiology and function. J Musculoskelet Neuronal Interact. 2004;4(2):199-201.
53. Barrack RL, Bruckner JD, Kneisl J, Inman WS, Alexander AH. The outcome of nonoperatively treated complete tears of the anterior cruciate ligament in active young adults. Clin Orthop Relat Res. 1990(259):192-9.

54. Fetto JF, Marshall JL. The natural history and diagnosis of anterior cruciate ligament insufficiency. Clin Orthop Relat Res. 1980(147):29-38.
55. Taylor DC, Posner M, Curl WW, Feagin JA. Isolated tears of the anterior cruciate ligament: over 30-year follow-up of patients treated with arthrotomy and primary repair. Am J Sports Med. 2009;37(1):65-71.
56. Murray MM, Spindler KP, Ballard P, Welch TP, Zurakowski D, Nanney LB. Enhanced histologic repair in a central wound in the anterior cruciate ligament with a collagen-platelet-rich plasma scaffold. J Orthop Res. 2007;25(8):1007-17.
57. Barlow Y, Willoughby J. Pathophysiology of soft tissue repair. Br Med Bull. 1992;48(3):698-711..
58. Tang Z, Yang L, Wang Y, Xue R, Zhang J, Huang W, et al. Contributions of different intraarticular tissues to the acute phase elevation of synovial fluid MMP-2 following rat ACL rupture. J Orthop Res. 2009;27(2):243-8.
59. Beynnon BD, Johnson RJ, Abate JA, Fleming BC, Nichols CE. Treatment of anterior cruciate ligament injuries, part I. Am J Sports Med. 2005;33(10):1579-602.
60. Eitzen I, Moksnes H, Snyder-Mackler L, Engebretsen L, Risberg MA. Functional tests should be accentuated more in the decision for ACL reconstruction. Knee Surg Sports Traumatol Arthrosc. 2010;18(11):1517-25.
61. Paterno MV. Non-operative Care of the Patient with an ACL-Deficient Knee. Curr Rev Musculoskelet Med. 2017;10(3):322-7.
62. Bogunovic L, Matava MJ. Operative and nonoperative treatment options for ACL tears in the adult patient: a conceptual review. Phys Sportsmed. 2013;41(4):33-40.
63. van der List JP, Hagemans FJA, Hofstee DJ, Jonkers FJ. The Role of Patient Characteristics in the Success of Nonoperative Treatment of Anterior Cruciate Ligament Injuries. Am J Sports Med. 2020;48(7):1657-64.
64. Lin KM, Boyle C, Marom N, Marx RG. Graft Selection in Anterior Cruciate Ligament Reconstruction. Sports Med Arthrosc Rev. 2020;28(2):41-8.
65. Paschos NK, Howell SM. Anterior cruciate ligament reconstruction: principles of treatment. EFORT Open Rev. 2016;1(11):398-408.
66. Mahapatra P, Horriat S, Anand BS. Anterior cruciate ligament repair - past, present and future. J Exp Orthop. 2018;5(1):20.
67. van der List JP, DiFelice GS. Primary repair of the anterior cruciate ligament: A paradigm shift. Surgeon. 2017;15(3):161-8.
68. Vacanti JP, Langer R. Tissue engineering: the design and fabrication of living replacement devices for surgical reconstruction and transplantation. Lancet. 1999;354 Suppl 1:SI32-4.
69. Vacanti CA. The history of tissue engineering. J Cell Mol Med. 2006;10(3):569-76.
70. Ikada Y. Challenges in tissue engineering. J R Soc Interface. 2006;3(10):589-601.
71. Bernhofer LP, Seiberg M, Martin KM. The influence of the response of skin equivalent systems to topically applied consumer products by epithelial--mesenchymal interactions. Toxicol In Vitro. 1999;13(2):219-29.

72. Caddeo S, Boffito M, Sartori S. Tissue Engineering Approaches in the Design of Healthy and Pathological In Vitro Tissue Models. Front Bioeng Biotechnol. 2017;5:40.
73. Bhatia SN, Ingber DE. Microfluidic organs-on-chips. Nat Biotechnol. 2014;32(8):760-72.
74. Hasirci V, Hasirci N. Tissue Engineering and Regenerative Medicine. In: Hasirci V, Hasirci N, editors. Fundamentals of Biomaterials. New York, NY: Springer New York; 2018. p. 281-302.
75. Gomes ME, Reis RL. Tissue engineering: key elements and some trends. Macromol Biosci. 2004;4(8):737-42.
76. Vunjak-Novakovic G, Altman G, Horan R, Kaplan DL. Tissue engineering of ligaments. Annu Rev Biomed Eng. 2004;6:131-56.
77. Kim BS, Baez CE, Atala A. Biomaterials for tissue engineering. World J Urol. 2000;18(1):2-9.
78. Puskas JE, Chen Y. Biomedical application of commercial polymers and novel polyisobutylene-based thermoplastic elastomers for soft tissue replacement. Biomacromolecules. 2004;5(4):1141-54.
79. Parchi PD, Ciapini G, Paglialunga C, Giuntoli M, Picece C, Chiellini F, et al. Anterior Cruciate Ligament Reconstruction with LARS Artificial Ligament-Clinical Results after a Long-Term Follow-Up. Joints. 2018;6(2):75-9.
80. Batty LM, Norsworthy CJ, Lash NJ, Wasiak J, Richmond AK, Feller JA. Synthetic devices for reconstructive surgery of the cruciate ligaments: a systematic review. Arthroscopy. 2015;31(5):957-68.
81. Rangel A, Colaço L, Nguyen NT, Grosset J-F, Egles C, Migonney V. Adapting mechanical characterization of a biodegradable polymer to physiological approach of anterior cruciate ligament functions. IRBM. 2022;43(1):39–48.
82. Petrigliano FA, Arom GA, Nazemi AN, Yeranosian MG, Wu BM, McAllister DR. In vivo evaluation of electrospun polycaprolactone graft for anterior cruciate ligament engineering. Tissue Eng Part A. 2015;21(7-8):1228-36.
83. Cooper JA, Lu HH, Ko FK, Freeman JW, Laurencin CT. Fiber-based tissue-engineered scaffold for ligament replacement: design considerations and in vitro evaluation. Biomaterials. 2005;26(13):1523-32.
84. Barnes CP, Sell SA, Boland ED, Simpson DG, Bowlin GL. Nanofiber technology: designing the next generation of tissue engineering scaffolds. Adv Drug Deliv Rev. 2007;59(14):1413-33.
85. Gelse K, Poschl E, Aigner T. Collagens--structure, function, and biosynthesis. Adv Drug Deliv Rev. 2003;55(12):1531-46.
86. Wnek GE, Bowlin GL. Collagen. In: Encyclopedia of Biomaterials and Biomedical Engineering. 2nd ed. New York: M. Dekker, Inc.; 2004. p. 628–38.
87. Roeder BA, Kokini K, Sturgis JE, Robinson JP, Voytik-Harbin SL. Tensile mechanical properties of three-dimensional type I collagen extracellular matrices with varied microstructure. J Biomech Eng. 2002;124(2):214-22.
88. Ge Z, Yang F, Goh JC, Ramakrishna S, Lee EH. Biomaterials and scaffolds for ligament tissue engineering. J Biomed Mater Res A. 2006;77(3):639-52.
89. Kuo CK, Marturano JE, Tuan RS. Novel strategies in tendon and ligament tissue engineering: Advanced biomaterials and regeneration motifs. Sports Med Arthrosc Rehabil Ther Technol. 2010;2:20.

90. Altman GH, Diaz F, Jakuba C, Calabro T, Horan RL, Chen J, et al. Silk-based biomaterials. Biomaterials. 2003;24(3):401-16.
91. Koh L-D, Cheng Y, Teng C-P, Khin Y-W, Loh X-J, Tee S-Y, et al. Structures, mechanical properties and applications of silk fibroin materials. Progress in Polymer Science. 2015;46:86–110.
92. Alessandrino A, Marelli B, Arosio C, Fare S, Tanzi MC, Freddi G. Electrospun silk fibroin mats for tissue engineering. Engineering in Life Sciences. 2008;8(3):219–25.
93. Seo YK, Choi GM, Kwon SY, Lee HS, Park YS, Song KY, et al. The biocompatibility of silk scaffold for tissue engineered ligaments. Key Engineering Materials. 2007;342–343:73–6.
94. Jin HJ, Chen J, Karageorgiou V, Altman GH, Kaplan DL. Human bone marrow stromal cell responses on electrospun silk fibroin mats. Biomaterials. 2004;25(6):1039-47.
95. Nau T, Teuschl A. Ligament tissue engineering: The Anterior Cruciate Ligament. Organ Tissue Engineering. 2020;1–18.
96. Maghdouri-White Y, Petrova S, Sori N, Polk S, Wriggers H, Ogle R, et al. Electrospun silk–collagen scaffolds and BMP-13 for ligament and tendon repair and regeneration. Biomedical Physics & Engineering Express. 2018;4(2):025013.
97. Bhardwaj N, Kundu SC. Electrospinning: a fascinating fiber fabrication technique. Biotechnol Adv. 2010;28(3):325-47.
98. Rutledge GC, Fridrikh SV. Formation of fibers by electrospinning. Adv Drug Deliv Rev. 2007;59(14):1384-91.
99. Ma Z, Kotaki M, Inai R, Ramakrishna S. Potential of nanofiber matrix as tissue-engineering scaffolds. Tissue Engineering. 2005;11(1–2):101–9.
100. Hasan A, Memic A, Annabi N, Hossain M, Paul A, Dokmeci MR, et al. Electrospun scaffolds for tissue engineering of vascular grafts. Acta Biomater. 2014;10(1):11-25.
101. Torre M, Di Feo F, De Angelis G, Ruspantini I, Frustagli G, Chistolini P. ACL reconstruction by bone-patellar tendon-bone graft: Mechanical evaluation of the elastic modulus and failure modes. Journal of Orthopaedics and Traumatology. 2003;4(2):69–75.
102. Peppas NA, Hilt JZ, Khademhosseini A, Langer R. Hydrogels in biology and medicine: From molecular principles to bionanotechnology. Advanced Materials. 2006;18(11):1345–60.
103. Liu J, Li L, Suo H, Yan M, Yin J, Fu J. 3D printing of biomimetic multi-layered Gelma/Nha Scaffold for osteochondral defect repair. Materials & Design. 2019;171:107708.
104. Amirikia M, Shariatzadeh SMA, Jorsaraei SGA, Mehranjani MS. Auto-fluorescence of a silk fibroin-based scaffold and its interference with fluorophores in labeled cells. Eur Biophys J. 2018;47(5):573-81
105. Hart D, Gurney-Dunlop T, Leiter J, Longstaffe R, Eid AS, McRae S, et al. Biomechanics of hamstring tendon, quadriceps tendon, and bone–patellar tendon–bone grafts for Anterior Cruciate Ligament Reconstruction: A Cadaveric Study. European Journal of Orthopaedic Surgery & Traumatology. 2022;33(4):1067–74.
106. Nichol JW, Koshy ST, Bae H, Hwang CM, Yamanlar S, Khademhosseini A. Cell-laden microengineered gelatin methacrylate hydrogels. Biomaterials. 2010;31(21):5536–44.2010.03.064.

107. Ravikanth M, Soujanya P, Manjunath K, Saraswathi T, Ramachandran C. Heterogenecity of fibroblasts. Journal of Oral and Maxillofacial Pathology. 2011;15(2):247.

8 CURRICULUM VITAE